Naval Research Laboratory

AD-A198 998

Approximate Calculation of Low Forward Speed Ship Radiation and Diffraction Wave Patterns

HENRY T. WANG

Center for Fluid/Structure Interactions
Laboratory for Computational Physics and Fluid Dynamics

August 26, 1988

88 9 28 045

REPORT DOCUMENTATION PAGE

Form Approved
OMB No 0704-0188

1a REPORT SECURITY CLASSIFICATION UNCLASSIFIED			1b RESTRICTIVE MARKINGS			
2a SECURITY CLASSIFICATION AUTHORITY			3 DISTRIBUTION / AVAILABILITY OF REPORT			
2b DECLASSIFICATION / DOWNGRADING SCHEDULE			Approved for public release; distribution unlimited.			
4 PERFORMING ORGANIZATION REPORT NUMBER(S) NRL Memorandum Report 6161			5 MONITORING ORGANIZATION REPORT NUMBER(S)			
6a NAME OF PERFORMING ORGANIZATION Naval Research Laboratory	6b OFFICE SYMBOL (If applicable) Code 4420		7a NAME OF MONITORING ORGANIZATION			
6c ADDRESS (City, State, and ZIP Code) Washington, DC 20375-5000			7b ADDRESS (City, State, and ZIP Code)			
8a NAME OF FUNDING / SPONSORING ORGANIZATION Office of Naval Research	8b OFFICE SYMBOL (If applicable)		9 PROCUREMENT INSTRUMENT IDENTIFICATION NUMBER			

8c ADDRESS (City, State, and ZIP Code) Arlington, VA 22217	10 SOURCE OF FUNDING NUMBERS			
	PROGRAM ELEMENT NO 61153N	PROJECT NO	TASK NO RR023-01-41	WORK UNIT ACCESSION NO DN158-017

11 TITLE (Include Security Classification)
Approximate Calculation of Low Forward Speed Ship Radiation and Diffraction Wave Patterns

12 PERSONAL AUTHOR(S)
Wang, Henry T.

13a TYPE OF REPORT Interim	13b TIME COVERED FROM 3/87 TO 10/87	14 DATE OF REPORT (Year, Month, Day) 1988 August 26	15 PAGE COUNT 46

16 SUPPLEMENTARY NOTATION

17	COSATI CODES		18 SUBJECT TERMS (Continue on reverse if necessary and identify by block number)
FIELD	GROUP	SUB-GROUP	Low forward speed Random sea waves
			Ship radiation and diffraction waves
			Far field spatial realizations (mpm)

19 ABSTRACT (Continue on reverse if necessary and identify by block number)

The present work generalizes a previous procedure for calculating the far field radiation and diffraction waves for a ship at zero speed in the presence of a random sea, to the low forward speed case. The far field waves are calculated by using a Green's function which accounts for linearized terms of the forward speed but neglects higher order terms. This results in a drastic simplification of the arbitrary speed case but retains some of the principal features of forward speed.

Extensive calculations are presented for the elevations and slopes of the ship, sea, and superposed waves for various cases of forward speed and sea state. The results are presented in the form of three-dimensional and contour plots. The results show that the effect of forward speed is to increase the magnitudes of the ship waves. Also, forward speed tends to destroy the near symmetry in the ship waves for bow and quartering seas, observed for the zero speed case.

20 DISTRIBUTION / AVAILABILITY OF ABSTRACT ☒ UNCLASSIFIED / UNLIMITED ☐ SAME AS RPT ☐ DTIC USERS	21 ABSTRACT SECURITY CLASSIFICATION UNCLASSIFIED	
22a NAME OF RESPONSIBLE INDIVIDUAL Henry T. Wang	22b TELEPHONE (Include Area Code) (202) 767-2516	22c OFFICE SYMBOL Code 4420

DD Form 1473, JUN 86   Previous editions are obsolete   SECURITY CLASSIFICATION OF THIS PAGE

S/N 0102-LF-014-6603

CONTENTS

APPROXIMATE CALCULATION OF LOW FORWARD SPEED
SHIP RADIATION AND DIFFRACTION WAVE PATTERNS

1. INTRODUCTION

In recent years, with the introduction of remote sensing systems such as Synthetic Aperture Radar (SAR), infrared (IR) and microwave (MR) radiometry, there has been considerable interest in assessing the detectability of ship generated waves in the presence of ambient ocean waves. Thus, the present author has conducted comparisons (with typical random ocean waves) of the Kelvin waves due to a nonoscillating ship traveling at constant forward speed in the spatial [1] and spectral [2] domains, and of the waves due to a ship at zero forward speed excited by the ocean waves in the spatial domain [3]. The ship waves have been calculated by using far field asymptotic approximations of the Green's functions for the Kelvin wake [4] and zero speed [5] cases. In complementary studies using more accurate near field formulations, the Kelvin wake has been calculated by using elementary infinite fluid Rankine [6] and the more complex free surface Kelvin [7] sources.

In all of the above studies, the ship waves have been calculated for the zero speed or zero frequency limits of the more general case of an oscillating, translating ship. The principal reason is due to the well known considerable increase in the complexity of the Green's function for the general case [8,9,10]. To the author's knowledge, there has been no extensive calculation of the actual ship waves for this general case. Using an ingenious approach, whereby the ship forward speed is considered to be small enough so that its squares may be systematically neglected, Grekas [11,12] derives a low speed Green's function which is considerably simpler than the corresponding function for arbitrary speed. He goes on to obtain a relatively simple far field asymptotic expression. This approach is used here, along with the formulation given in [3], to calculate a series of approximate spatial realizations of wave elevations and slopes generated by a low speed ship excited by typical ambient ocean waves. As in [3], realizations are also calculated for the random sea waves and superposed sea and ship waves to assess the detectability of the ship waves.

The report starts by describing Grekas's approach. In particular, the behavior of his far field expression as a function of the dimensionless parameter $U\omega/g$ (where U is the ship forward speed, ω is the circular oscillation frequency, and g is the gravity constant) is discussed in detail. The procedure previously used in [3] for generalizing the far field expression, which is for a single source oscillating at a single frequency, to the case of the multiple sources modeling the ship hull and the multiple frequencies and headings modeling the random sea, is briefly summarized. Modifications of this procedure, which is for zero speed, to account for the present case of low forward speeds, are outlined. Spatial realizations of ship waves, sea waves, and superposed waves for Sea States 2, 5, and 8 are presented in the form of three-dimensional and contour plots. The detectability of the ship waves are discussed as a function of sea state, the type of realization (elevation or slope), the form of presentation (three-dimensional or contour) and the upper bound assigned to the parameter $U\omega/g$. The report concludes with a summary of the major findings.

2. THEORETICAL FORMULATION FOR SINGLE SOURCE

2.1 Low Speed Green's Function

For a submerged pulsating source in the presence of a uniform current in the x-direction, shown in Fig. 1, the Green's function G must satisfy the following well known free surface condition

$$\frac{\partial^2 G}{\partial t^2} + 2U \frac{\partial^2 G}{\partial x \partial t} + U^2 \frac{\partial^2 G}{\partial x^2} + g \frac{\partial G}{\partial z} = 0 \text{ on } z = 0. \tag{1}$$

1

If the strength Q of the pulsating source is taken to vary with time as a simple harmonic function

$$Q = \text{Re}(Q^* e^{-i\omega t})$$ (2)

where Re denotes taking the real part, then G can be expressed by

$$G = G_1(x, y, z; x', y', z') e^{-i\omega t}.$$ (3)

Equation (1) can then be rewritten in terms of spatial variables as follows

$$-\omega^2 G_1 - 2Ui\omega \frac{\partial G_1}{\partial x} + U^2 \frac{\partial^2 G_1}{\partial x^2} + g \frac{\partial G_1}{\partial z} = 0 \text{ on } z = 0.$$ (4)

It is well known that the Green's function satisfying Eq. (4) is troublesome to evaluate [8]. One of the principal difficulties is that Eq. (4) gives a higher order pole appearing in the denominator in integral representations of G_1.

To minimize these difficulties, Grekas [11,12] makes the crucial assumption that the velocity U is sufficiently small so that U^2 may be neglected in Eq. (4), resulting in the following simpler free surface condition

$$-\omega^2 G_2 - 2Ui\omega \frac{\partial G_2}{\partial x} + g \frac{\partial G_2}{\partial z} = 0 \text{ on } z = 0.$$ (5)

The resulting Green's function G_2, which now has only a simple pole, represents a drastic simplification of the more general function G_1. The detailed derivation given in [11], and summarized in [13], will not be repeated here.

By using the principle of stationary phase, Grekas goes on to obtain the following relatively simple algebraic expression for the far field values of G_2

$$G_2 = \frac{Q^*}{i} \frac{g}{2\pi\sqrt{R}} f(\theta_0) \sqrt{\frac{2\pi}{g''(\theta_0)}} e^{i[k_0(\theta_0)R\cos(\theta_0 - \gamma) + k_0 z' - \pi/4]}$$ (6)

where

$$R = \sqrt{(x - x')^2 + (y - y')^2}$$ (7a)

θ is the wave propagation direction

$\gamma = \tan^{-1}(y - y')/(x - x')$ is the spatial direction (7b)

$$f(\theta_0) = \frac{k_0 e^{k_0 z'}}{g + 2\omega U \cos \theta_0}$$ (7c)

$$k_0 = \frac{\omega_0^2}{g} = \frac{(\omega - U k_0 \cos \theta_0)^2}{g} \approx \frac{\omega^2}{g + 2U'\omega \cos \theta_0}$$ (7d)

2

is the wavenumber in terms of the intrinsic circular frequency ω_0

$$g''(\theta_0) = \frac{-g \cos(\theta_0 - \gamma)\omega^2}{(g + 2\omega U \cos\theta_0)^2} \tag{7e}$$

θ_0 is the root of the $\theta - \gamma$ relationship given by

$$g'(\theta_0) = g \sin(\gamma - \theta_0) + 2\omega U \sin\gamma = 0. \tag{7f}$$

It should be pointed out that the expression for $g''(\theta_0)$ in [11] is erroneously raised to a power of 3 instead of 2.

One check on the accuracy of the above expression is to consider the case when U is set equal to zero. By noting that in this case

$$\gamma \equiv \theta_0 \equiv \theta \tag{8a}$$

$$k_0 = \frac{\omega_0^2}{g} \equiv \frac{\omega^2}{g} = k \tag{8b}$$

G_2 for $U = 0$ becomes

$$G_0 = G_2 (U = 0) = \frac{Q^*}{4\pi i} 2\pi \sqrt{\frac{2k}{\pi R}} e^{i(kR + k' - \pi/4)}. \tag{9}$$

This is identical to the far field expression for the zero speed Green's function given in [5,8].

One indication of the simplicity of the low speed function is that, similar to the $U = 0$ case, for a given spatial direction γ there is one and only one wave, whose direction of propagation θ_0 is given by Eq. (7f). The difference is that for $U = 0$, $\theta_0 \equiv \gamma$, which leads to a set of circular ring waves which are centered around the source. These simple waves may be compared to the more complicated Kelvin wake which has zero or two waves depending on γ, and the waves due to G_1 which have zero to five waves depending on γ and $U\omega/g$.

In the present work, it is not the Green's function itself, but the elevation ζ and x and y slopes ζ_x and ζ_y which are of interest. Keeping only the terms which are linear in G_2 in the Bernouilli equation, the elevation ζ due to a single pulsating source is given by

$$\zeta = \text{Re} \left\{ -\frac{1}{g} \left[\frac{\partial G_2}{\partial t} + U \frac{\partial G_2}{\partial x} \right] = \frac{i\omega}{g} G_2 - \frac{iU}{g} \frac{\partial G_2}{\partial x} \right\}. \tag{10}$$

Taking $\partial/\partial x$ of G_2 given by Eq. (6) would, in general, involve the following three factors: $1/\sqrt{R}$, $g''(\theta_0)$, and $\exp[ik_0 R \cos(\theta_0 - \gamma)]$. However, taking $\partial/\partial x$ of the first two factors gives higher powers of R in the denominator which may be neglected in the far field. In taking $\partial/\partial x$ of the exponential term, it is of interest to note the following relationship

$$R \cos(\theta_0 - \beta) = (x - x') \cos\theta_0 + (y - y') \sin\theta_0. \tag{11}$$

3

The derivative $\partial/\partial x$ of the exponential term is then simply given by

$$\frac{\partial}{\partial x} \, e^{ik_0 R \cos(\theta_0 - \beta)} = ik_0 \cos \theta_0 \, e^{ik_0 R \cos(\theta_0 - \beta)}. \tag{12}$$

Using Eqs. (6), (10), and (12), the elevation ζ is then given by

$$\zeta = \mathrm{Re} \, \frac{i}{g} \, [(\omega - U k_0 \cos \theta_0) \, G_2]. \tag{13}$$

The slopes ζ_x and ζ_y are conveniently obtained from ζ by again using Eq. (11)

$$\zeta_x = \frac{\partial}{\partial x} \, \zeta = \mathrm{Re} \, (ik_0 \cos\theta_0 \zeta) \tag{14a}$$

$$\zeta_y = \frac{\partial}{\partial y} \, \zeta = \mathrm{Re} \, (ik_0 \sin \theta_0 \, \zeta). \tag{14b}$$

Figures 2a, b, and c respectively show sample plots of ζ calculated by using Eq. (13) for $U = 0$, $U < 0$ (directed in the -x direction), and $U > 0$. Figure 2a shows the expected circular ring waves which are symmetrical in all four quadrants, while Figs. 2b and 2c show that in the case of $|U| > 0$, symmetry is preserved only in the lateral y direction. In the x direction, the crests tend to be dense upstream and sparse downstream, in accordance with the sketch given by Grekas [11,12].

2.2 Significance of the Parameter $\nu = U\omega/g$

Grekas points out that his formulation is valid only for

$$\left[\nu = \frac{U\omega}{g}\right] < \frac{1}{2}. \tag{15}$$

This can be seen from Eq. (7d) which shows that the wave number $k_0 - \infty (\lambda - 0)$ as $\nu \to 1/2$, as well as from Eqs. (7e) and (6) which show that $g'' \to 0$ (and hence $G_2 \to \infty$) as $\nu \to \frac{1}{2}$. Figures 3a to 3e give three-dimensional plots which show the manner in which the maximum wave amplitudes ζ_M increase and the upstream wavelengths decrease as ν increases from 0 to 0.49. Figure 3e shows that for $\nu = 0.49$, the chosen grid is not fine enough to model the short wavelengths and the upstream region is plotted as a plateau. Table 1 shows the variation of the ratio ζ_M/ζ_{M0}, where ζ_{M0} is the value of ζ_M for the $U = 0$ case, for values of ν between 0 and 0.49.

The above shows that it is important to place an upper limit on ν, ν_U, to prevent unrealistically large values of ζ. (For example, it is shown later that for typical sea states, it is always possible to make the ship generated waves dominate the ocean waves by choosing ν_U sufficiently close to the singular limit of 0.5.) Basically, it is of interest to choose a value of ν_U which is large enough to give an indication of the effect of U, without giving excessively large elevations. It was decided to make most of the calculations of the ship waves using a value of $\nu_U = 0.25$. It may be noted that this value lies halfway between the possible limits of 0 and 0.5, and that at this value the maximum elevation is approximately three times that of the $U = 0$ case (see Table 1), which represents a moderate but appreciable modification. Also, it is well known that for the case of the general Green's function G_1 (for arbitrary values of U) the character of the wave patterns changes at this value of ν.

4

3. THEORETICAL FORMULATION FOR SHIP AND SEA WAVES

To obtain the ship waves, the above formulation for the elevation of a single source oscillating at a single frequency must be generalized to the multiple sources modeling the ship hull, and the multiple frequencies and headings modeling a random sea. The first section describes the procedure used to model the random sea, the following section summarizes the previously used method [3] to generate ship waves at zero forward speed, the third section describes the modifications implemented to account for the present case of low speed, and the last section briefly describes how the wave slopes are obtained from the elevations.

The coordinate system used in the present work to calculate the ship and sea waves coincides with that used in the Ship Motion Program SMP [14] and is shown in Fig. 4. It should be noted that the x axis is directed forward, from stern to bow. Thus, the ship forward speed in this coordinate system corresponds to a flow in the -x direction for the coordinate system for the single pulsating source, shown in Fig. 1.

3.1 Random Sea Wave Elevations

As was done in [3], the random sea elevations $\zeta_{SE}(x, y, t)$ are approximated by a double sum over wave number k_m and wave heading μ_n of sinusoidal components, as follows

$$\zeta_{SE} = \text{Re} \sum_{m=1}^{M} \sum_{n=1}^{N} \alpha_{mn} \, e^{i\phi_{mn}} e^{i[k_m(x\cos\mu_n + y\sin\mu_n) - \omega_m t]} = \text{Re} \sum_{m=1}^{M} \sum_{n=1}^{N} \zeta_{SEmn} \tag{16}$$

where

$$\alpha_{mn} = \sqrt{2S(\omega_m)\Delta\omega} \, \sqrt{G(\mu_n)\Delta\mu} = \alpha_m \alpha_n \tag{17a}$$

$S(\omega_m)$ is the value of the frequency spectrum at wave frequency ω_m.

$G(\mu_n)$ is the value of the spreading function at wave heading μ_n, taken

relative to the wind direction β_W

$$\mu_n = \beta_n - \beta_W \tag{17b}$$

β_n is the wave heading measured with respect to the x axis

$\Delta\omega$ and $\Delta\mu$ are increments in ω and μ.

In the present work, the frequency spectrum is taken to be that of Pierson-Moskowitz, while the spreading function is taken to be the commonly used cosine squared function

$$G(\mu) = \frac{2}{\pi} \cos^2 \mu, \quad \frac{-\pi}{2} \leq \mu \leq \frac{\pi}{2}. \tag{18}$$

As was done in [3], five values of ω are taken so as to give equal values of α_m, while 13 equally spaced values of μ between $-\pi/2$ and $\pi/2$ are used.

3.2 Zero Speed Ship Radiation and Diffraction Waves

Radiation waves refer to those generated by the six oscillatory modes of motion of the ship (three symmetric or vertical modes, and three antisymmetric or lateral modes) shown in Fig. 4, while diffraction waves refer to the scattering of the incident wave by the ship hull (one symmetric, one antisymmetric). The resultant ship radiation and diffraction waves ζ_{SH} in the presence of a random sea are expressed in [3] by the following triple sum over the ($M = 5$) sea frequencies, ($N = 13$) sea headings, and 8 ship oscillation modes

$$\zeta_{SH} = \mathrm{Re} \sum_{m=1}^{M} \sum_{n=1}^{N} \sum_{j=1}^{8} \zeta_{SHmnj} = \mathrm{Re} \sum_{m=1}^{M} \sum_{n=1}^{N} \alpha_{mn} e^{i\phi_{mn}} \sum_{j=1}^{8} T_j \zeta_j \tag{19}$$

where $T_j (\omega, \beta)$ is the complex motion response transfer function calculated by SMP for the six radiation modes, $j = 1, \ldots, 6$, and $T_7 \equiv T_8 \equiv (1., 0.)$ for the symmetric and antisymmetric diffraction modes, $j = 7, 8$. The variable ζ_j represents the wave elevation for unit amplitude for the jth ship oscillation mode and is given by

$$\zeta_j = \mathrm{Re} \left[\frac{-1}{4\pi} \frac{\omega}{g} \bar{H}_j (k, \theta) (G_0 e^{-i\omega t}) \right] \tag{20}$$

where G_0 is the Green's function for $U = 0$ given in Eq. (9). $\bar{H}_j$ is the complex conjugate of the Kochin function H_j

$$H_j(k, \theta) = -\iint_S \gamma_j (x', y', z') e^{[kz' + ik(x'\cos\theta + y'\sin\theta)]} dS \tag{21}$$

where γ_j is the hull surface distribution of singularity strengths calculated by SMP for the jth radiation mode, $j = 1, \ldots, 6$; x', y', z' are respectively the x, y, z coordinates of the source located on the hull surface. The Kochin functions for the diffraction modes H_7 (symmetric) and H_8 (antisymmetric) are obtained by taking the singularity strengths to be a function of wave heading β, as follows

$$\gamma_7 = -\gamma_3 e^{-ikx'\cos\beta} \tag{22a}$$

$$\gamma_8 = i \sin \beta \, \gamma_2 \, e^{ikx'\cos\beta} \tag{22b}$$

3.3 Modifications for Low Forward Speed

The above formulation must be modified in a number of ways in the case of forward speed. In view of the approximation of low speed in the derivation of G_2, Eq. (6), and the further uncertainity in choosing proper values of the parameter ν in this equation, these modifications will be kept to a minimum. The intent is to model the major features of forward speed, while keeping the overall formulation as simple as possible.

The modifications are basically centered about the expression for ζ_j given in Eq. (20). It is well known that in the case of forward speed U, the radiation waves ($j = 1, \ldots, 6$) occur at the

encounter frequency ω_e which is related to wave frequency ω and heading β by

$$\omega_e = \omega \left| 1 - \frac{\omega U}{g} \cos \beta \right| \qquad j = 1, \ldots, 6 \qquad (23a)$$

whereas the diffraction waves ($j = 7,8$) are not affected by U, i.e.,

$$\omega_e = \omega \qquad j = 7, 8. \qquad (23b)$$

The second modification consists of expressing the elevation in terms of G_2 instead of G_0, by using Eq. (13) as follows

$$\frac{\omega}{g} G_0 \rightarrow \left[\frac{\omega_e}{g} - \frac{U'}{g} k_0 \cos \theta_0 \right] G_2 (U') \qquad (24)$$

where $U' = -U$ to account for the previously mentioned difference in direction of flow between SMP (Fig. 4) and the single source formulation (Fig. 1).

Strictly speaking, the Kochin functions H_j and motion transfer coefficients T_j for the radiation modes $j = 1, \ldots, 6$ should be calculated for the encounter frequencies ω_e. Since there are 13 headings and five frequencies, this would mean the use of 65 sets of H_j and T_j. For the sake of convenience, the previously calculated values of H_j and T_j for the zero speed case [3] are also used in the present work. In addition to the already mentioned approximate nature of the forward speed Green's function used here, the results of [15] indicate that the motion coefficients at low speeds vary relatively slowly with speed. Also, as shown later, the diffraction waves ($j = 7, 8$), for which the singularity distribution for zero speed is correct, tend to be larger than the radiation waves. Thus, the present approximation qualitatively preserves the major effects of forward speed.

Combining Eqs. (23), (24), and the preceding remarks, the low speed equivalents for the zero speed single mode and total ship waves, respectively given by Eqs. (20) and (19), become

$$\zeta_j = \text{Re} \left[\frac{-1}{4\pi} \left[\frac{\omega_e}{g} - \frac{U'}{g} k_0 \cos \theta_0 \right] \bar{H}_j (k, \theta) (G_2 e^{-i\omega_e t}) \right] \qquad (25)$$

$$\zeta_{SH} = \text{Re} \sum_{m=1}^{M} \sum_{n=1}^{N} \sum_{j=1}^{8} \zeta_{SHmnj} = \text{Re} \sum_{m=1}^{M} \sum_{n=1}^{N} \alpha_{mn} e^{i\phi_{mn}} \sum_{j=1}^{8} T_j (\omega, \beta) \zeta_j . \qquad (26)$$

3.4 Wave Slopes

As shown in Eq. (14), wave slopes are conveniently obtained by multiplying the elevations by the wavenumbers in the desired horizontal direction. The wave slopes in the x and y directions for the sea waves ζ_{SE} (Eq. 16), ship waves ζ_{SH} (Eq. 26), and superposed waves ζ_T, are simply given by the following sums

$$\zeta_{SEx} = \text{Re} \sum_{m=1}^{M} \sum_{n=1}^{N} ik_m \cos \mu_n \zeta_{SEmn} \qquad (27a)$$

$$\zeta_{SEy} = \text{Re} \sum_{m=1}^{M} \sum_{n=1}^{N} ik_m \sin \mu_n \zeta_{SEmn} \qquad (27b)$$

7

$$\zeta_{SHx} = \text{Re} \sum_{m=1}^{M} \sum_{n=1}^{N} \sum_{j=1}^{8} ik_{0mj} \cos \theta_{0mj} \; \zeta_{SHmnj} \tag{28a}$$

$$\zeta_{SHy} = \text{Re} \sum_{m=1}^{M} \sum_{n=1}^{N} \sum_{j=1}^{8} ik_{0mj} \sin \theta_{0mj} \; \zeta_{SHmnj} \tag{28b}$$

$$\zeta_{Tx} = \zeta_{SEx} + \zeta_{SHx}$$

$$= \text{Re} \sum_{m=1}^{M} \sum_{n=1}^{N} i \; (k_m \cos \mu_n \; \zeta_{SEmn} + \sum_{j=1}^{8} k_{0mj} \cos \theta_{0mj} \; \zeta_{SHmnj}) \tag{29a}$$

$$\zeta_{Ty} = \zeta_{SEy} + \zeta_{SHy}$$

$$= \text{Re} \sum_{m=1}^{M} \sum_{n=1}^{N} i (k_m \sin \mu_n \zeta_{SEmn} + \sum_{j=1}^{8} k_{0mj} \sin \theta_{0mj} \; \zeta_{SHmnj} \tag{29b}$$

where

$$k_m = \frac{\omega_m^2}{g}$$

$$k_{0mj} = \frac{\omega_{emj}^2}{g + 2U' \cos \theta_{0mj} \omega_{emj}}$$

θ_{omj} is given by $g \sin(\gamma - \theta_{0mj}) + 2\omega_{emj} \, U' \sin \gamma = 0$

ω_{emj} is defined by Eqs. (23a) and (23b).

4. COMPUTER CALCULATIONS

4.1 Computer Program

The previously used code for zero speed [3] has been revised to account for low forward speed. The program accepts from one input file data on the speed and direction of the wind, the frequency spectrum to be used, the number of frequency components, the types of waves to be calculated (ship, sea, or total of ship and sea; elevation, x slope, or y slope) and the ship speed. In this same file are specified data for the rectangular grid over which the waves are calculated: its origin, and the number and spacing of the points along the (x', y') axes, which are inclined at angle α to the (x, y) system (see Fig. 5). As a second input file, the program accepts the Kochin functions $H_j(\omega, \theta, \beta)$ and transfer functions $T_j(\omega, \beta)$ calculated by SMP [14].

The program then performs the calculations for the wave elevations and slopes given by Eqs. (16)-(29). The calculated waves are saved as an output plot file from which three-dimensional or contour plots may be generated. Examples of these plots are given in the following chapter.

8

4.2 Adaptation of Formulation to SMP Results

SMP calculates the functions H_j and T_j for 30 discrete values of ω between 0.2 and 2.4 rad/sec, and 13 equally spaced values of θ and β between 0 and 180 degrees. Thus, it is of interest to describe the procedure used to model the general case of values of ω, β, and θ which may not coincide with, or fall outside the range of, the SMP results. This procedure is described in detail in [3], and is briefly summarized here.

In order to more accurately model the lower sea states, where the higher ω's are of interest, the two highest frequencies calculated by SMP were changed from 2.2 and 2.4 to 2.4 and 2.8 rad/sec, respectively. This essentially consisted of changing one DATA statement in SMP. The values of H_j and T_j are approximated by those corresponding to the SMP values of ω which come closest to the actual values.

The wave headings β are taken to be the 13 equally spaced headings between 0 and 180 degrees used in SMP. Noting that the energy of the wind is spread 90 degrees on either side of the wind direction (see Eq. (18)), the SMP formulation is most conveniently used when the wind direction β_W is 90 degrees, i.e., in this case the wave headings of interest are simply the 0 to 180 degree cases considered by SMP. For other wind directions, not all 13 values considered by SMP are used, and negative values of β are involved. In these cases, use is made of the fact that for the vertical modes $(j = 1, 3, 5, 7)$ $T_j(\omega, -\beta) \equiv T_j(\omega, \beta)$ while for the lateral modes $(j = 2, 4, 6, 8)$ $T_j(\omega, -\beta) \equiv -T_j(\omega, \beta)$, i.e.,

$$T_j(\omega, -\beta) = (-1)^{j+1} T_j(\omega, \beta) \qquad j = 1, 2, \ldots, 7, 8. \tag{30}$$

The Kochin functions H_j are defined only for 13 positive values of θ evenly spaced between 0 and 180 degrees. For arbitrary positive values of θ, the value of H_j is obtained by simple interpolation. For negative values of θ, H_j is obtained by noting that the ship waves are symmetrical with respect to θ for the vertical modes and antisymmetric for the lateral modes, i.e.,

$$H_j(-\theta) = (-1)^{j+1} H_j(\theta) \qquad j = 1, 2, \ldots, 7, 8. \tag{31}$$

4.3 Computer Runs

In view of the approximations made in the present work, it is not felt that the theory can effectively differentiate ship hulls of different shape. Thus, all runs were made using the DE1006 as the sample hull. This ship has a length L of 308 ft, a beam B of 35.9 ft, and a draft H of 12.1 ft.

Three Sea States were considered: 2, 5, and 8, which respectively correspond to wind speeds of 12, 24, and 42 knots. Table 2 shows the five frequencies ω and associated wavelengths λ chosen to model each Sea State. This table shows that the ranges of λ's for Sea State 2, 5, and 8 are respectively smaller than, include, and larger than the ship length L. Most of the runs were made for a wind heading β_W of 45 degrees, which corresponds to quartering seas. To illustrate the effect of heading on the ship waves, runs were also made where heading varied between 0 and 180 degrees. Two values of U were considered in the computer runs: $U = 0$ and $U = 10$ knots (16.88 ft/s), which gives the Froude number $F_n = 0.17$ where

$$F_n = \frac{U}{\sqrt{gL}}. \tag{32}$$

9

5. CALCULATED SEA AND SHIP WAVE PATTERNS

5.1 Random Sea Elevations and Slopes

Figures 6 and 7 show plots of the random sea elevations and slopes. These are given for illustrative purposes as well as for comparison with the ship generated waves shown later in this chapter. Figures 6a, b, and c respectively show three-dimensional plots of the elevations for Sea States 2, 5, and 8, while Figs. 6d-f show the corresponding contour plots for these Sea States. Figures 7a and b respectively show three-dimensional plots of the x and y slopes for Sea State 5, while Figs. 7c and d show the corresponding contour plots.

The wind direction β_W is taken to be 45 degrees, the quartering sea case. The wave patterns are calculated for a square x-y grid given by

$$0 \leq x, y \leq 4\lambda_0 \tag{33}$$

where λ_0 is the longest wavelength, corresponding to the fundamental frequency ω_0, shown for each Sea State in Table 2.

5.2 Effect of ν_U on Ship Waves

It was previously shown in Fig. 3 the manner in which the wave elevations for a single source become singular as the upper limit of ν, ν_U, approaches 0.5. As a result, it was pointed out that ν_U is taken equal to 0.25 in most of the ship wave calculations. Figures 8a and b show, for the case of Sea State 8, $\beta_W = 45$ degrees, $U = 10$ knots, three-dimensional plots of the ship waves ζ_{SH} and the superposed ship and sea waves ζ_T, for the square grid defined by Eq. (33) for a choice of $\nu_U = 0$. Figs. 8c-f show corresponding pairs of plots for choices of $\nu_U = 0.25$ and 0.45.

Figures 8b and d show that for $\nu_U \leq 0.25$, there is little visual difference between the superposed waves ζ_T and the sea waves ζ_{SE} shown in Fig. 6c for Sea State 8. When ν_U increases to 0.45, Figs. 8e and f show that ζ_T now show features which are clearly those of ζ_{SH}. Results for $\nu_U = 0.49$, which are not presented, show that ζ_{SH} becomes so large that it is virtually indistinguishable from ζ_T. Thus, similar to the single source case, the ship waves can be made arbitrarily large by choosing ν_U arbitrarily close to 0.50. In all subsequent ship waves shown in this chapter, the intermediate value of 0.25 is used.

5.3 Effect of Forward Speed U

Figures 9a-d show three-dimensional plots of the ship wave elevations ζ_{SH} for Sea State 5, $\beta_W = 45$ deg, as U increases from 0 to 20 knots (33.76 ft/s). The elevations are plotted for a rectangular grid which now shows the waves aft as well as forward of the ship

$$-4\lambda_0 \leq x \leq 4\lambda_0, \quad 0 \leq y \leq 4\lambda_0. \tag{34}$$

The figure shows how the upstream waves tend to cluster and the downstream waves tend to disperse beyond the end of the grid as U increases. Due to the adopting of the upper limit of 0.25 on $\nu = U\omega/g$, Figs. 9c and d show that there is relatively little change in both the pattern and amplitude of the ship waves for $U \geq 6$ knots (10.13 ft/s).

5.4 Effect of Wind Heading β_W

Figures 10a and b show three-dimensional plots of the ship waves for Sea State 5, $U = 0$, over the rectangular grid defined in Eq. (34), for values of β_W equal to 45 and 135 deg. Figures 11a and b show corresponding results for $U = 10$ knots. Figure 10 shows that for $U = 0$ the strongest waves are those which are diffracted approximately at the same angle as β_W, and there is a certain symmetry between the plots for β_W and $180\text{-}\beta_W$. Due to the upstream clustering and downstream dispersion of the waves, Fig. 11 shows that no such symmetry exists in the forward speed case. Results for $\beta_W = 0$ and 180 deg show a similar trend. Thus, for wind headings of 0 and 45 deg, most of the waves are clustered upstream. On the other hand, for the corresponding wind headings of 180 and 135 deg, the ship waves fill the entire calculation grid.

5.5 Decomposition of Ship Waves Into Radiation and Diffraction Components

For Sea State 5 with $\beta_W = 45$ deg, $U = 10$ knots, and the square calculation grid given by Eq. (33), Figs. 12a to c respectively show three-dimensional plots of the resultant ship waves ζ_{SH}, and the radiation and diffraction components, ζ_{SHR} and ζ_{SHD}. Recall that ζ_{SHR} refers to the sum over $j = 1, \ldots, 6$ and ζ_{SHD} refers to the sum over $j = 7, 8$ of the expression for ζ_{SH} given by Eqs. (19) or (26).

This figure clearly shows that the major contribution to the resultant ship waves is made by the diffraction component. Similar results hold for other Sea States and values of U. This tends to justify the simplification discussed in Section 3.3 of using the zero speed Kochin functions, which is appropriate only for the diffraction waves. This figure also shows the expected trend of the diffraction waves being more directional than the radiation waves.

5.6 Comparison of Superposed and Sea Waves

For $\beta_W = 45$ deg, $U = 0$, and the square calculation grid given by Eq. (33), Fig. 13a shows the three-dimensional plot of the superposed wave elevations ζ_T for Sea State 2, while Figs. 13b and c show the corresponding plots for $U = 10$ knots for Sea States 2 and 5. Figures 14a to c show contour plots of these same elevations. Figures 15a and b respectively show three-dimensional plots of the x and y slopes of the superposed waves for Sea State 5 for $U = 0$, while Figs. 15c and d show the plots for the $U = 10$ knots case. Finally, Figs. 16a and b show the corresponding contour plots of the $U = 0$ case given in Figs. 15a and b.

The superposed waves in the above figures may be compared to the ocean waves shown in Figs. 6 and 7. In the case of the three-dimensional plot for $U = 0$, Fig. 13a shows that even in the case of Sea State 2, for which diffraction effects dominate, the superposed waves are only moderately different from the corresponding sea waves shown in Fig. 6a. The plots of the superposed waves for Sea States 5 and 8 are virtually indistinguishable from the corresponding sea waves, and hence have not been shown. In the case of $U = 10$ knots, for which the ship waves are larger, Fig. 13b shows that in the case of Sea State 2, the superposed waves are completely different from the sea waves while the differences are small but now perceptible for Sea State 5. The same observations hold in comparing the contour plots of the superposed waves in Figs. 14a to c with the corresponding sea waves shown in Figs. 6d and e. In all cases, the trend for Sea State 8 is similar to that of Sea State 5.

In view of the small differences between the superposed and sea wave elevations for the higher Sea States, it is of interest to compare the wave slopes. In the case of three-dimensional plots for Sea State 5, Figures 15a and b show that the x and y slopes of the superposed waves are only slightly different from the corresponding sea wave slopes shown in Figs. 7a and b. On the other hand, for

11

$U = 10$ knots, Figs. 15c and d show that there are substantial differences in the case of the x slope and moderate differences in the case of the y slope. The larger differences for the x slope are due to the previously mentioned wave clustering in the upstream direction, which leads to shorter wavelengths. The near lack of difference between the three-dimensional plots of the wave slopes for $U = 0$ makes it of interest to further consider the corresponding contour plots. Figure 16a shows that the differences are very small for the x slope, but noticeable for the y slope. While not shown, a similar difference exists in the y slope at $U = 0$ for Sea State 8.

6. SUMMARY

A previously derived formulation for calculating ship generated radiation and diffraction waves has been generalized to the case of low forward speed. One modification consists of replacing the previously used far field Green's function for zero speed by a low forward speed function, for which all terms involving the square of speed are considered negligible. It is shown that this new function retains the previous simplicity of one set of waves everywhere, with the difference that the wave propagation direction no longer coincides with the spatial direction of the field point. The manner in which the wavelengths decrease and wave amplitudes increase is shown as the singular limit of 0.5 is approached for the parameter $\nu = U\omega/g$, where U is the forward speed and ω is the circular frequency. For an upper bound on ν, ν_U, equal to 0.25, the maximum wave amplitude is approximately three times as large as that of the zero speed case. A second modification to the zero speed case consists of replacing the sea wave frequencies by frequencies of encounter for the radiation modes.

A series of three-dimensional and contour plots are given for the sea, ship, and superposed sea and ship wave elevations and slopes for the DE1006 ship in the presence of Sea States 2, 5, and 8. It is again shown that by choosing ν_U arbitrarily close to 0.5 the ship waves can always be made to dominate the sea waves. The tendency for the upstream waves to cluster and the downstream waves to disperse as U increases is illustrated by a series of three-dimensional plots. For $U = 0$, there is a certain near symmetry between the ship waves for wind headings β_W and 180-β_W. For $U = 10$ knots, no such symmetry exists due to the above upstream clustering and downstream dispersion. For both $U = 0$ and 10 knots, the ship diffraction waves tend to dominate the radiation waves.

In comparing the superposed ship and sea waves with the corresponding sea waves alone, the plots for zero forward speed show little difference in the elevations and x slopes of these waves for Sea States 5 and 8, and moderate differences in the case of Sea State 2. It is only in the contour plots of the y slope that appreciable differences can be detected between the superposed and sea waves at the higher Sea States. In the case of $U = 10$ knots, for which the ship waves are larger, there now exist small (but perceptible) differences for the wave elevations, large differences in the x slope, and moderate differences in the y slope at the higher Sea States.

7. ACKNOWLEDGMENT

12

8. REFERENCES

1. Keramidas, G.A., Wang, H.T., Burke, J.A., and Bauman, W., "KELSEA: An Interactive Computer Code for Kelvin and Random Ambient Sea Waves," *Proceedings of the International Conference on Computer Aided Design, Manufacture and Operation in the Marine and Offshore Industries (CADMO 86)*, pp 411-423, September 1986.

2. Wang, H.T. and Rogers, J.C.W., "Spectral Comparisons of Ocean Waves and Ship Kelvin Wakes," *Proceedings of the Seventh (1988) International Offshore Mechanics and Arctic Engineering Symposium*, Vol. II, pp. 253-261, February 1988.

3. Wang, H.T., "Spatial Realizations of Ship Radiation and Diffraction Waves in Random Ambient Sea Waves," NRL Memorandum Report 5950, May 1987.

4. Eggers, K.W.H., Sharma, S.D., and Ward, L.W., "An Assessment of Some Experimental Methods for Determining the Wavemaking Characteristics of a Ship Form," *Transactions of the Society of Naval Architects and Marine Engineers*, Vol. 75, pp. 112-157, November 1967.

5. Liu, H.C., "Uber die Entstehung von Ringwellen an einer Flüssigkeitsoberfläche durch unter dieser gelegene, kugelige periodische Quellensysteme," *Zeitschrift für Angewandte Mathematik und Mechanik*, Vol. 32, pp. 211-226, July 1952.

6. Cheng, B.H., Dean, J.S., and Jayne, J.L., "The XYZ Free Surface Program and its Application to Transom-Stern Ships With Bow Domes," *Proceedings of the Second DTNSRDC Workshop on Ship Wave-Resistance Computations*, pp. 370-392, November 1983.

7. Telste, J.G., "Calculation of Wave Elevations in Ship Wakes by Using the SWIM Free-Surface (SWIMFS) Code," DTNSRDC Report 86/030, June 1986.

8. Wehausen, J.V. and Laitone, E.V., "Surface Waves," *Encyclopedia of Physics*, Vol. 9, Springer-Verlag, Berlin, pp. 446-778, 1960.

9. Bougis, J., "Etude de la Diffraction-Radiation dans le Cas d'un Flotteur Indéformable Animé d'une Vitesse Moyenne Constante et Sollicité par une Houle Sinusoidale de Faible Amplitude," Thèse de Docteur-Ingénieur, Université de Nantes, July 1980.

10. Haskind, M.D., "The Hydrodynamic Theory of Ship Oscillations in Sea Waves," *Prikladnaya Matematika i Mekhanika*, Vol. 10, pp. 33-66, 1946 (in Russian).

11. Grekas, A., "Contribution à l'Etude Théorique et Expérimentale des Efforts du Second Ordre et du Comportement Dynamique d'une Structure Marine Sollicitee par une Houle Regulière et un Courant," Thèse de Docteur-Ingénieur, Université de Nantes, July 1981.

12. Grekas, A., and Delhommeau, G., "Diffraction-radiation en présence d'un courant," *Bulletin de l'Association Technique Maritime et Aéronautique*, Vol. 83, pp. 293-319, 1983.

13. Wang, H.T., "Survey of European Studies on the Far Field Characteristics of a Source Oscillating and Translating Near a Free Surface," NRL Memorandum Report 6078, March 1988.

14. Meyers, W.G., Applebee, T.R., and Baitis, A.E., "User's Manual for the Standard Ship Motion Program, SMP," DTNSRDC Report SPD-0936-01, September 1981.

15. Frank, W. and Salvesen, N., "The Frank Close-Fit Ship-Motion Computer Program," NSRDC Report 3289, June 1970.

Table 1 — Variation of Maximum Amplitudes
ζ_M / ζ_{M0} with Values of $\nu = U\omega/g$

$\nu = U\omega/g$	ζ_M / ζ_{M0}
0.	1.
0.031	1.08
0.062	1.18
0.125	1.54
0.25	2.98
0.3	3.85
0.35	5.62
0.375	9.92
0.4	13.25
0.45	57.13
0.49	1,707.6

Table 2 — Wave Components
for Sea States 2, 5, and 8

ω(rad/sec)	λ(ft)
Sea State 2, V = 12 knots	
1.229	134
1.433	99
1.635	76
1.922	55
2.774	26
Sea State 5, V = 24 knots	
0.611	541
0.717	394
0.819	302
0.965	217
1.409	102
Sea State 8, V = 42 knots	
0.349	1,653
0.410	1,204
0.468	924
0.551	666
0.806	312
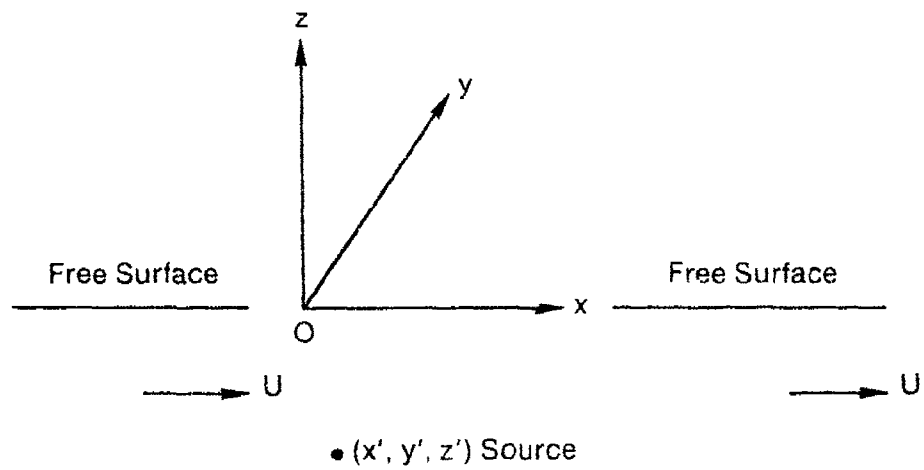
Fig. 1 — Definition of Grekas's coordinate system for single source

Fig. 2a — $U = 0$

Fig. 2b — $U < 0$
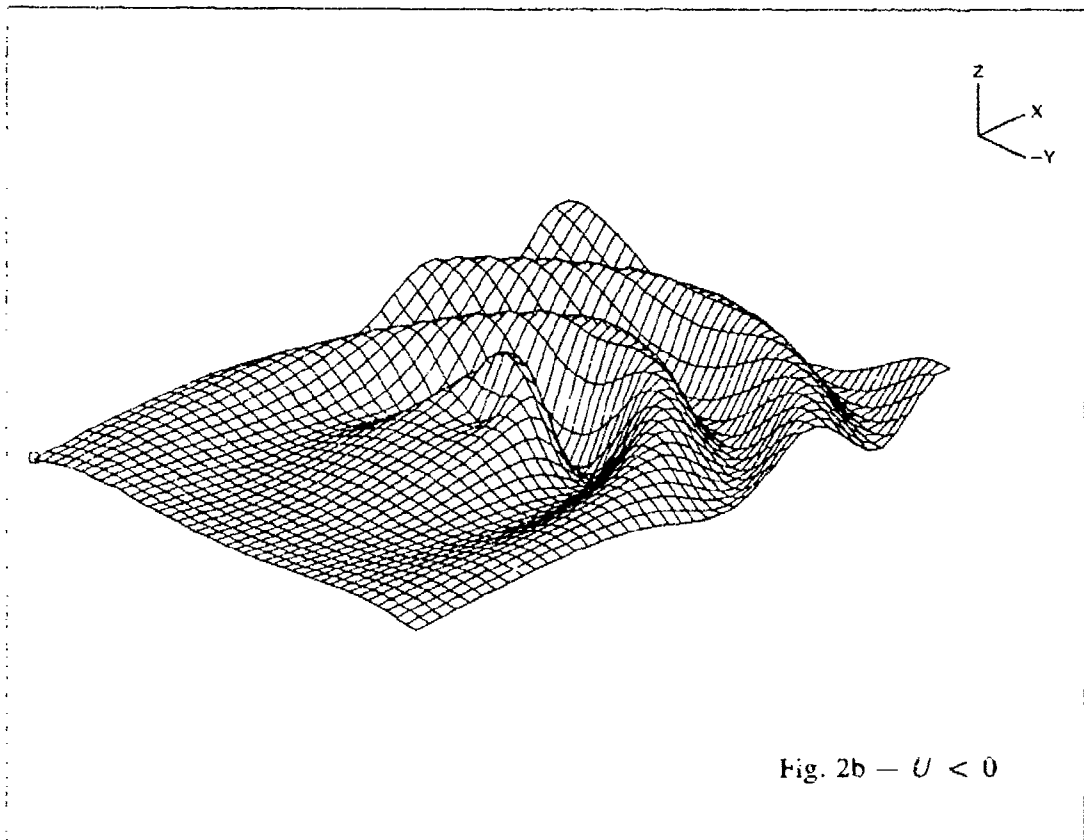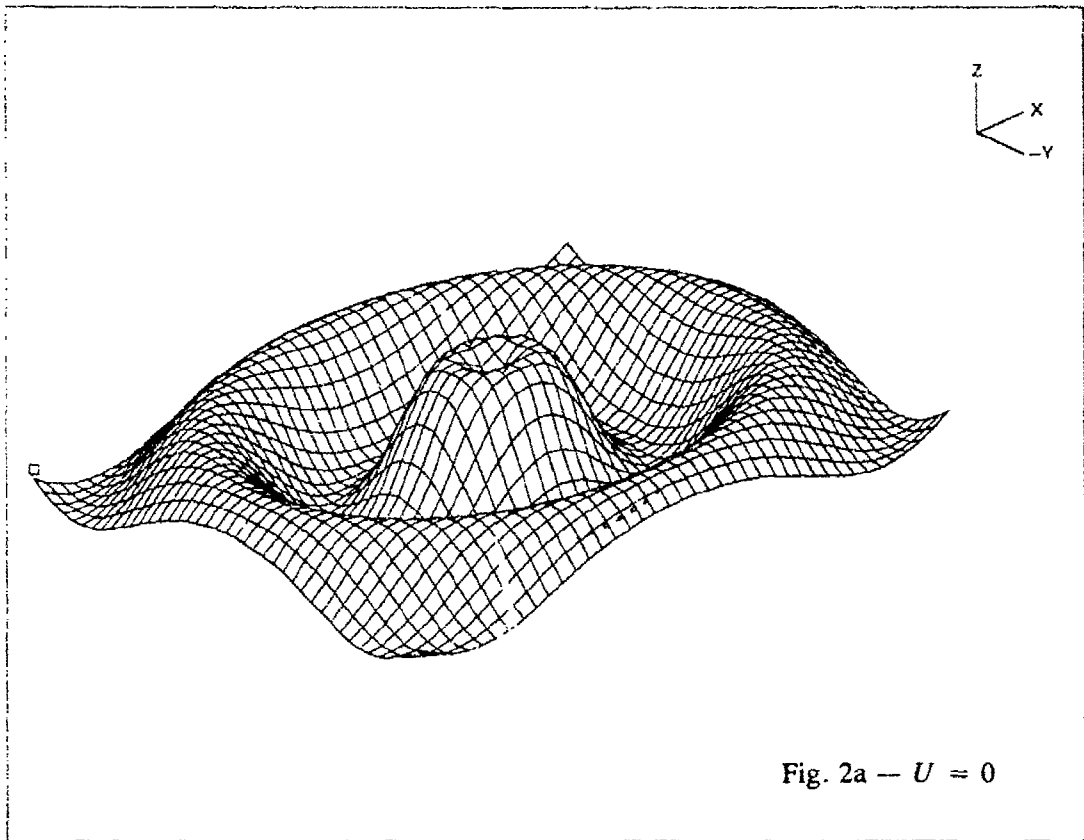
Fig. 2 — Sample wave patterns for single source for different cases of U

Fig. 2c — $U > 0$
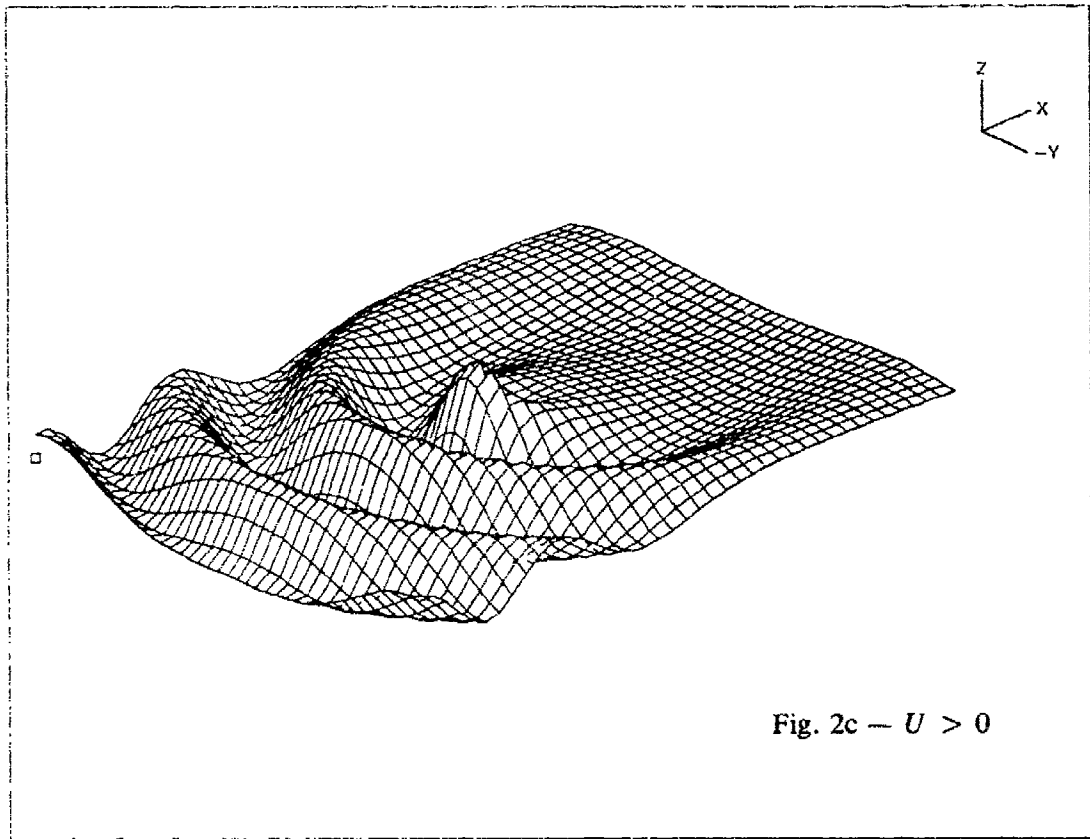
Fig. 2 (Continued) — Sample wave patterns for single source for different cases of U
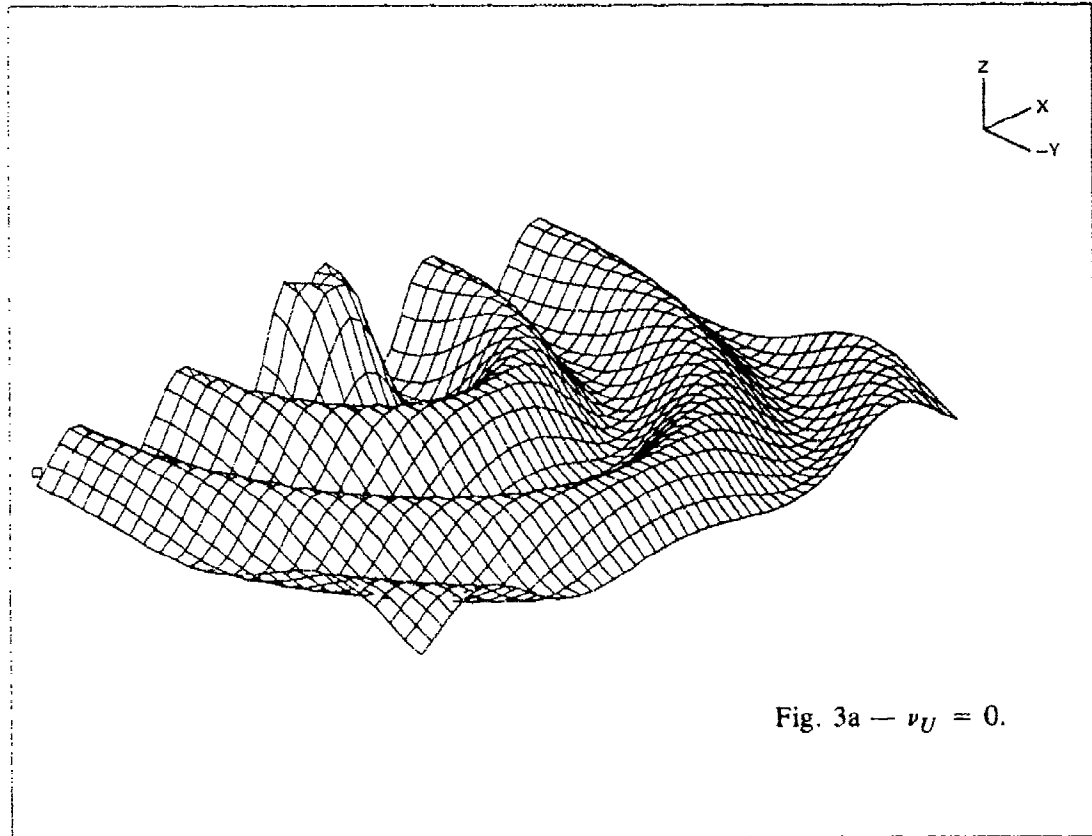
Fig. 3a — $\nu_U = 0.$

Fig. 3 — Sample wave patterns for single source for $U = 30$ ft/s, different values of ν_U
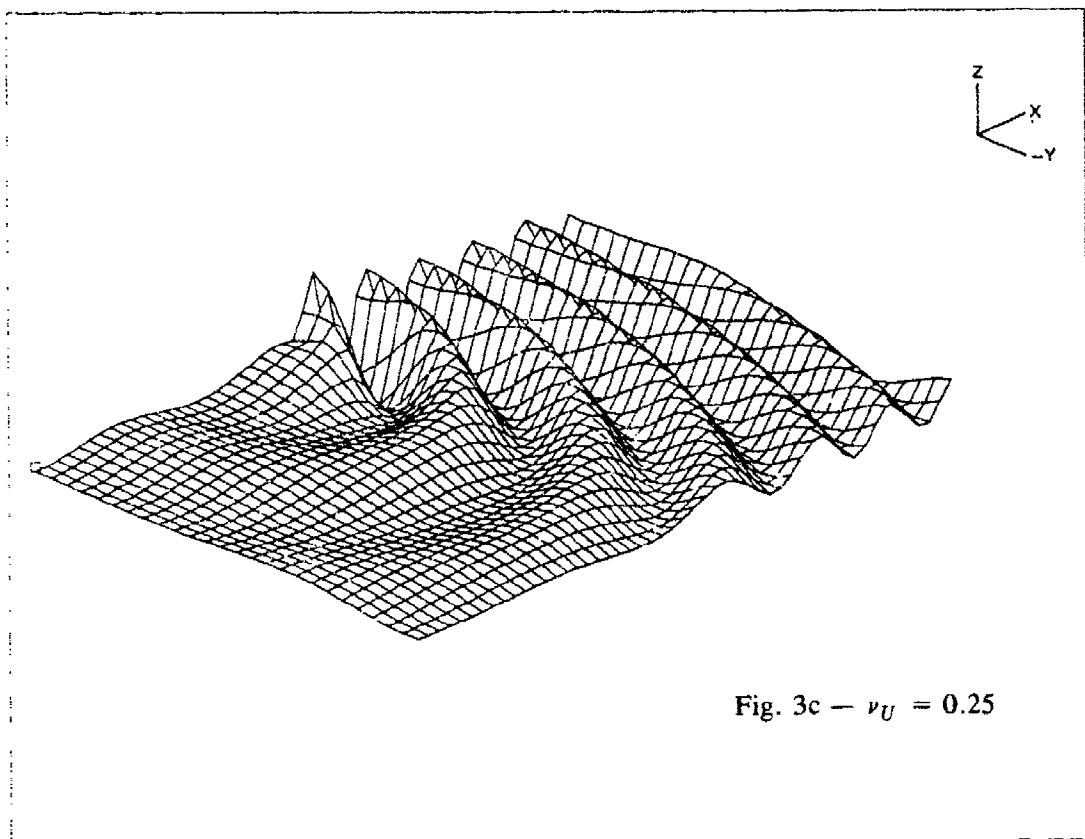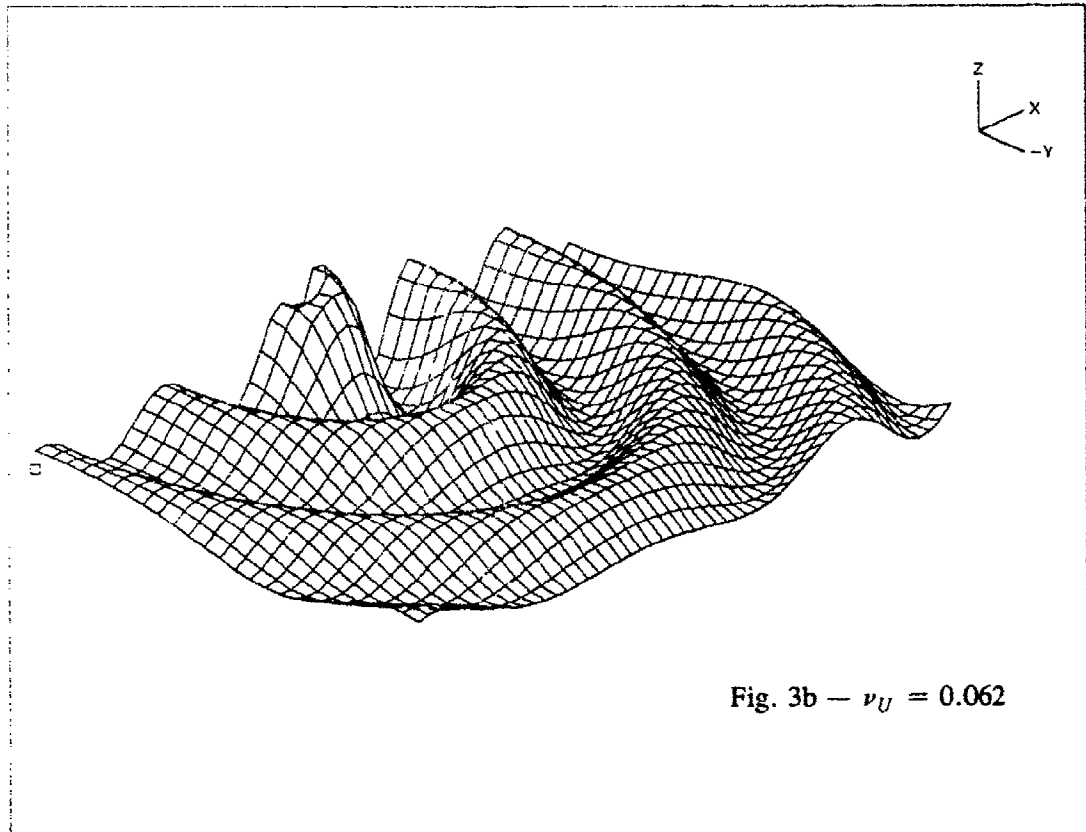
18

Fig. 3b — $\nu_U = 0.062$

Fig. 3c — $\nu_U = 0.25$

Fig. 3 (Continued) — Sample wave patterns for single source for $U = 30$ ft/s, different values of ν_U

Fig. 3d — $\nu_U = 0.40$

Fig. 3e — $\nu_U = 0.49$

Fig. 3 (Continued) — Sample wave patterns for single source for $U = 30$ ft/s, different values of ν_U

20

ξ_1 = SURGE $\quad\quad$ ξ_3 = HEAVE $\quad\quad$ ξ_5 = PITCH
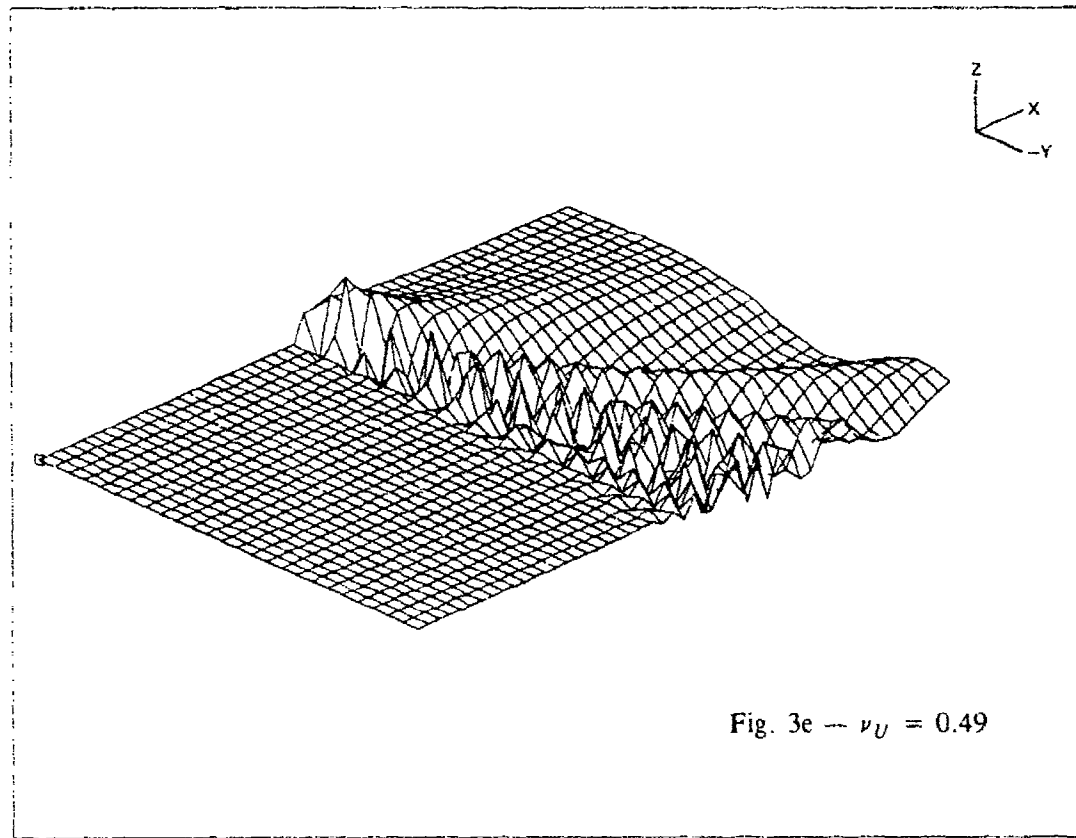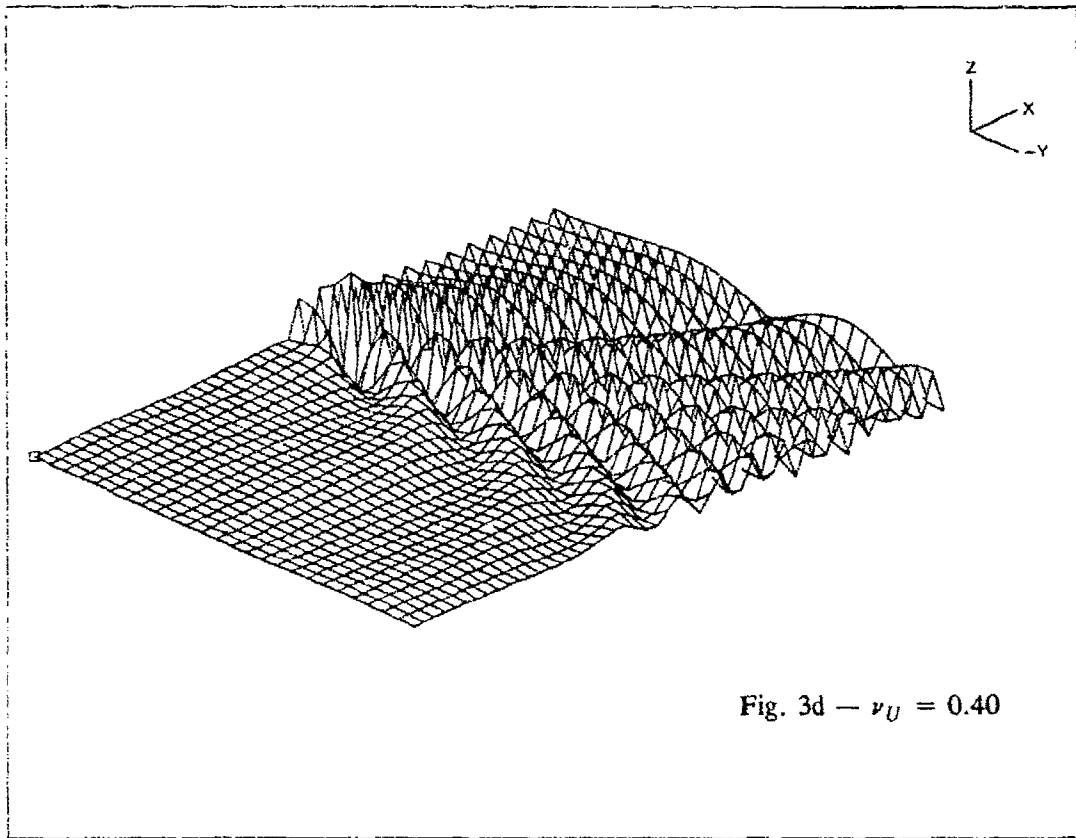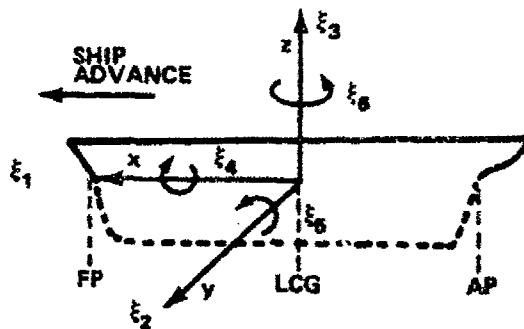
ξ_2 = SWAY $\quad\quad$ ξ_4 = ROLL $\quad\quad$ ξ_6 = YAW

Fig. 4 — Definition of Ship Motions Program coordinate system and modes of ship oscillation
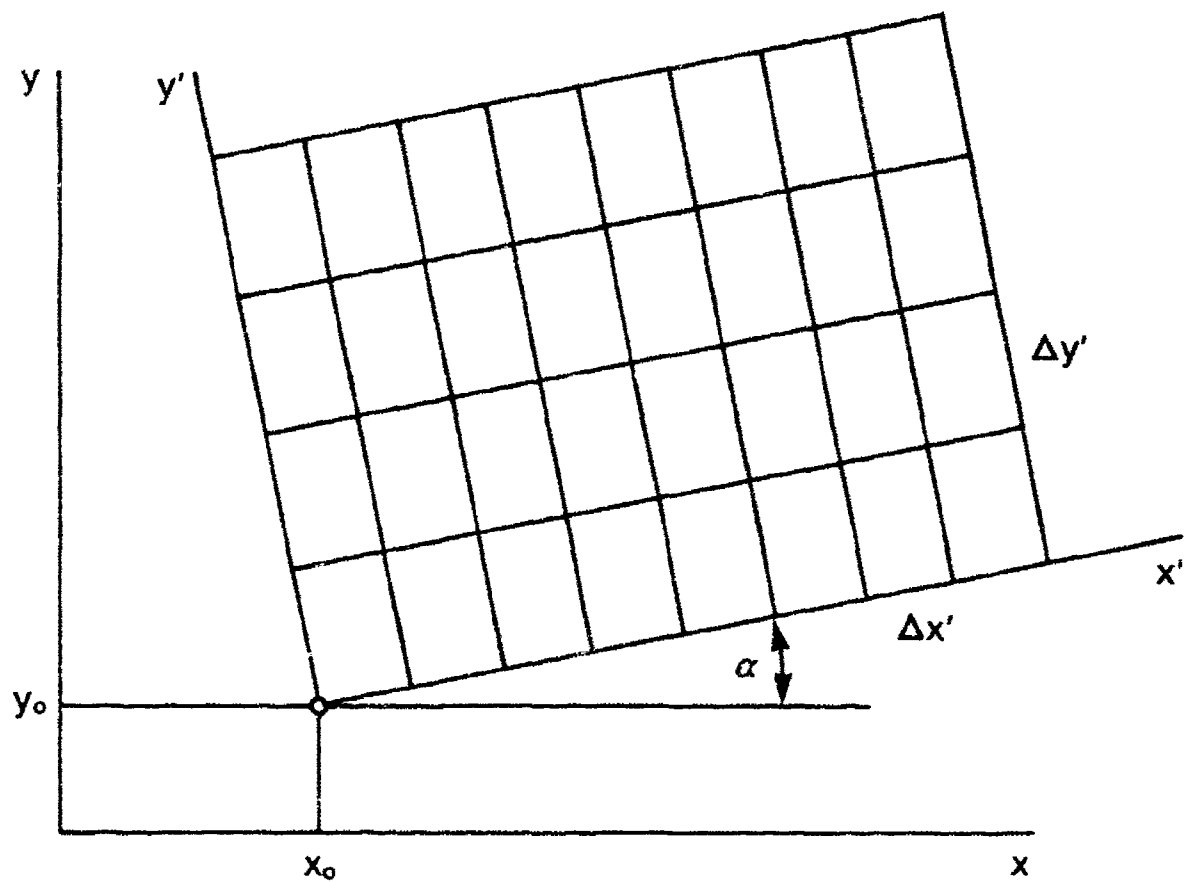
Fig. 5 — Definition of calculation grid

22
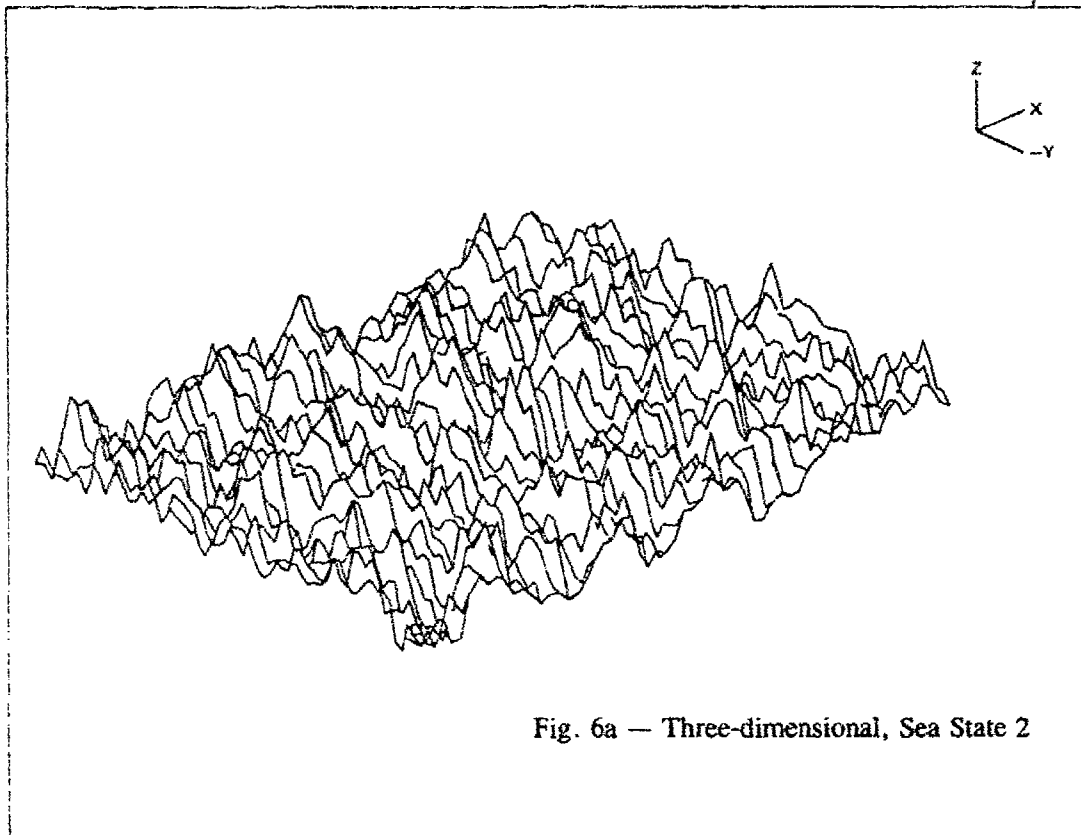
Fig. 6a — Three-dimensional, Sea State 2
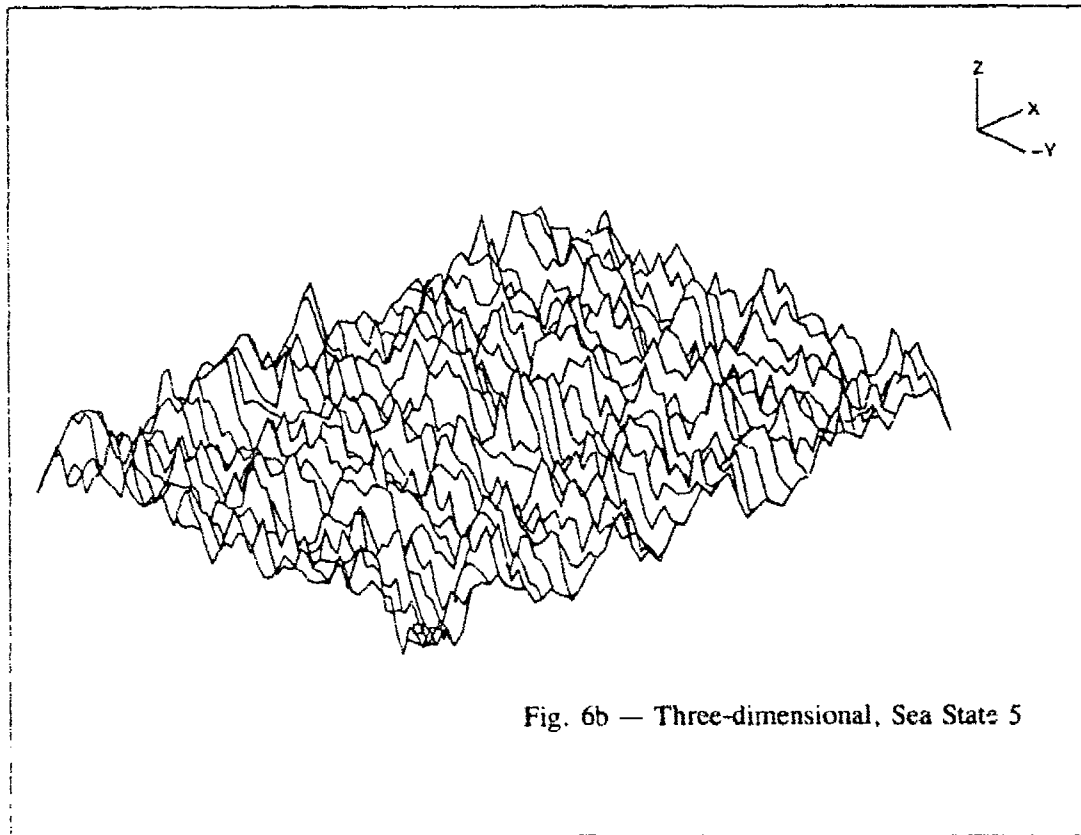
Fig. 6b — Three-dimensional, Sea State 5

Fig. 6 — Plots of random sea wave elevations, β_W = 45 degrees

Fig. 6c — Three-dimensional, Sea State 8

Fig. 6d — Contour, Sea State 2
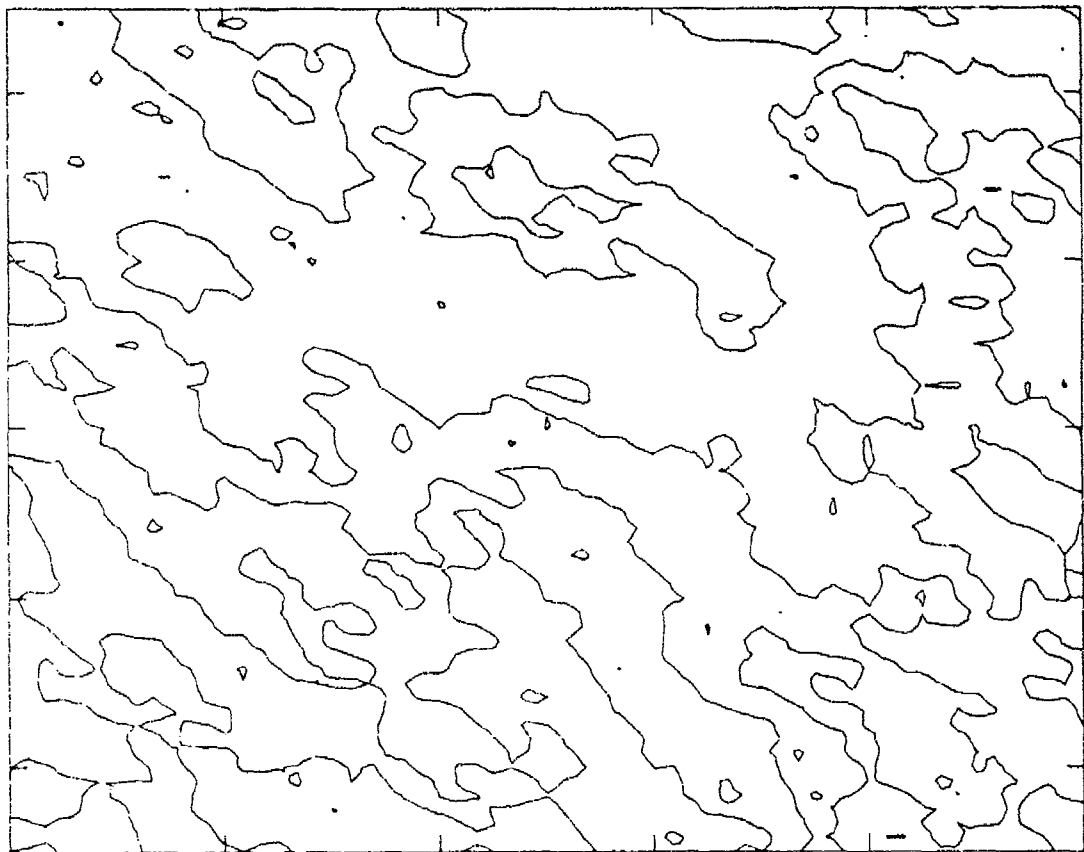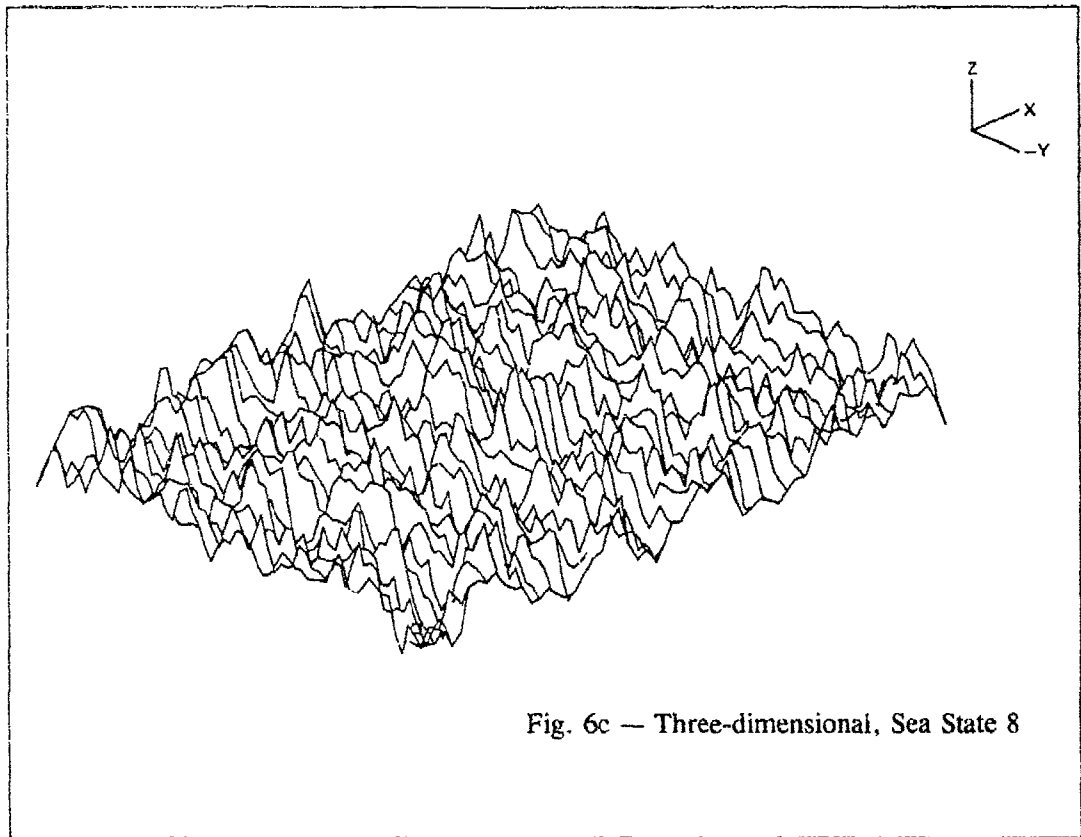
Fig. 6 (Continued) — Plots of random sea wave elevations, $\beta_W = 45$ degrees
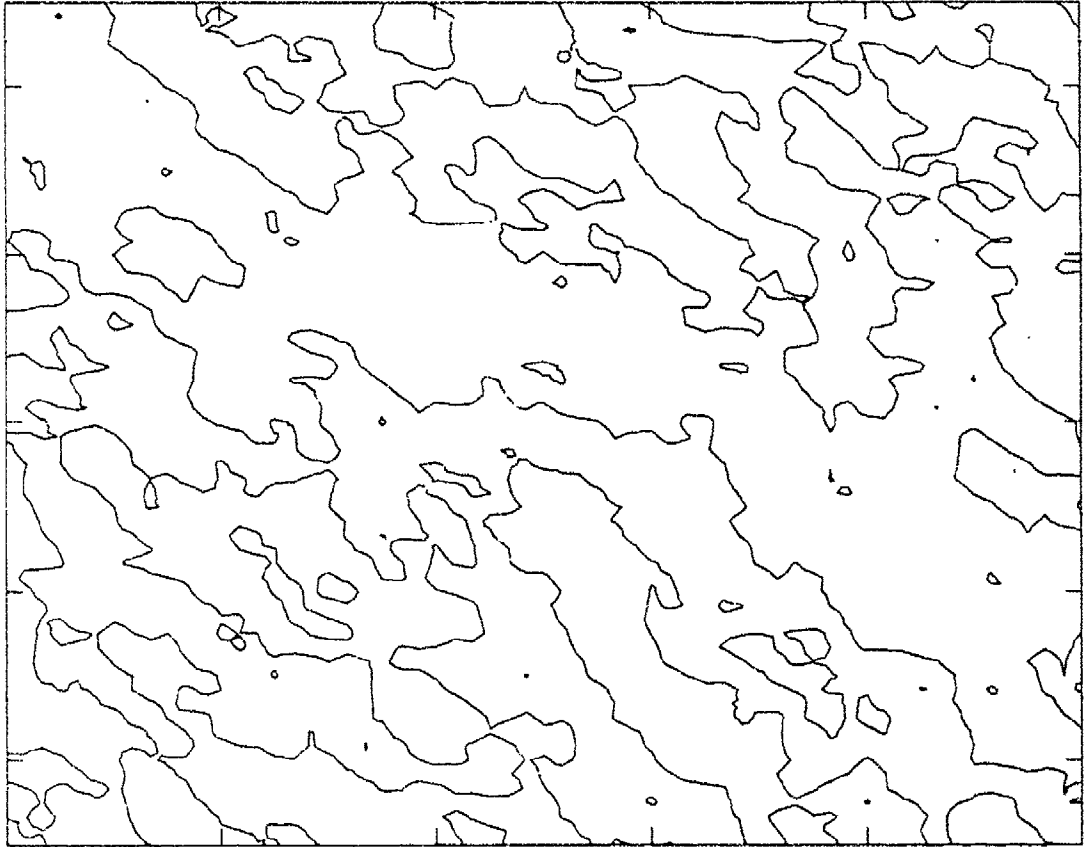
Fig. 6e — Contour, Sea State 5
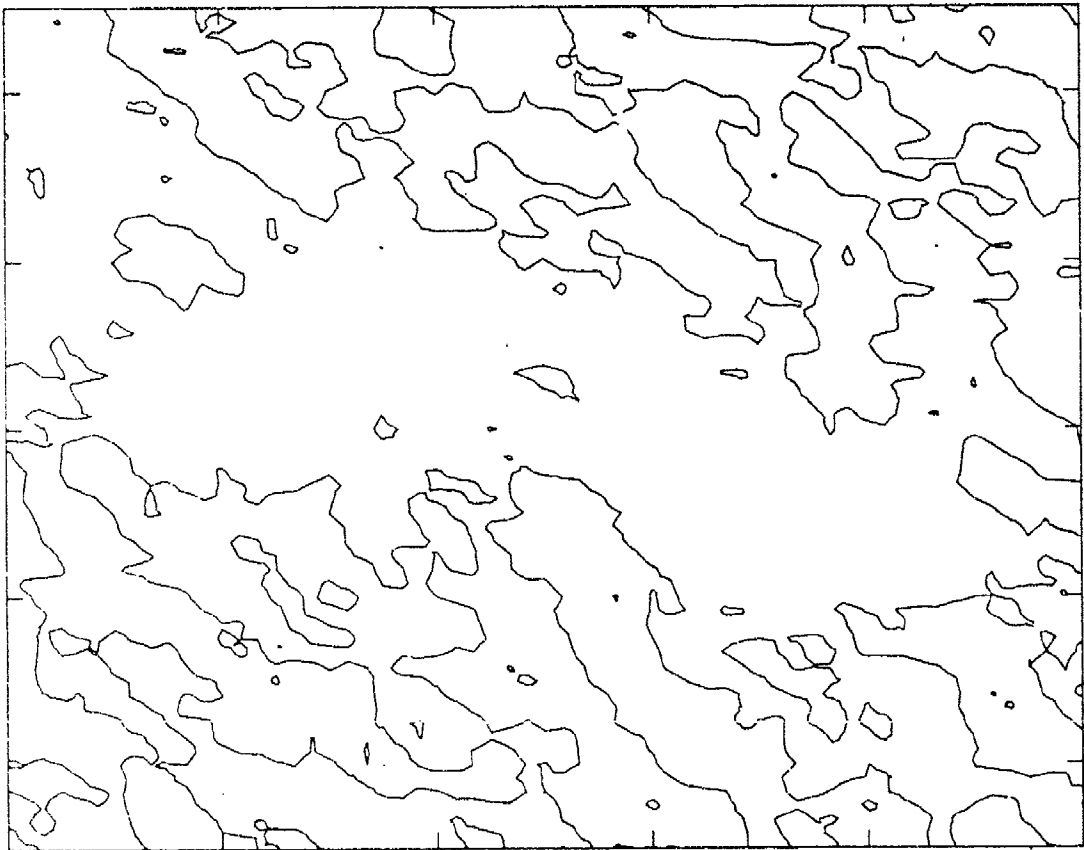
Fig. 6f — Contour, Sea State 8

Fig. 6 (Continued) — Plots of random sea wave elevations, $\beta_W = 45$ degrees
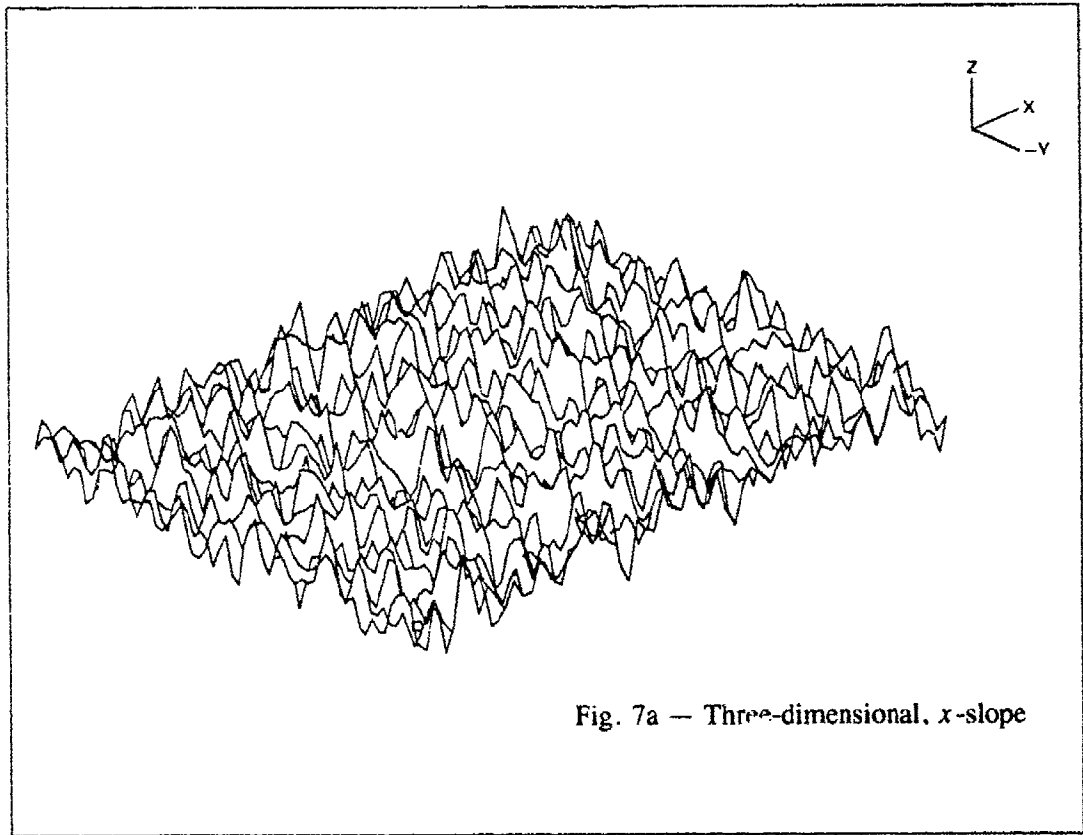
Fig. 7a — Three-dimensional, x-slope
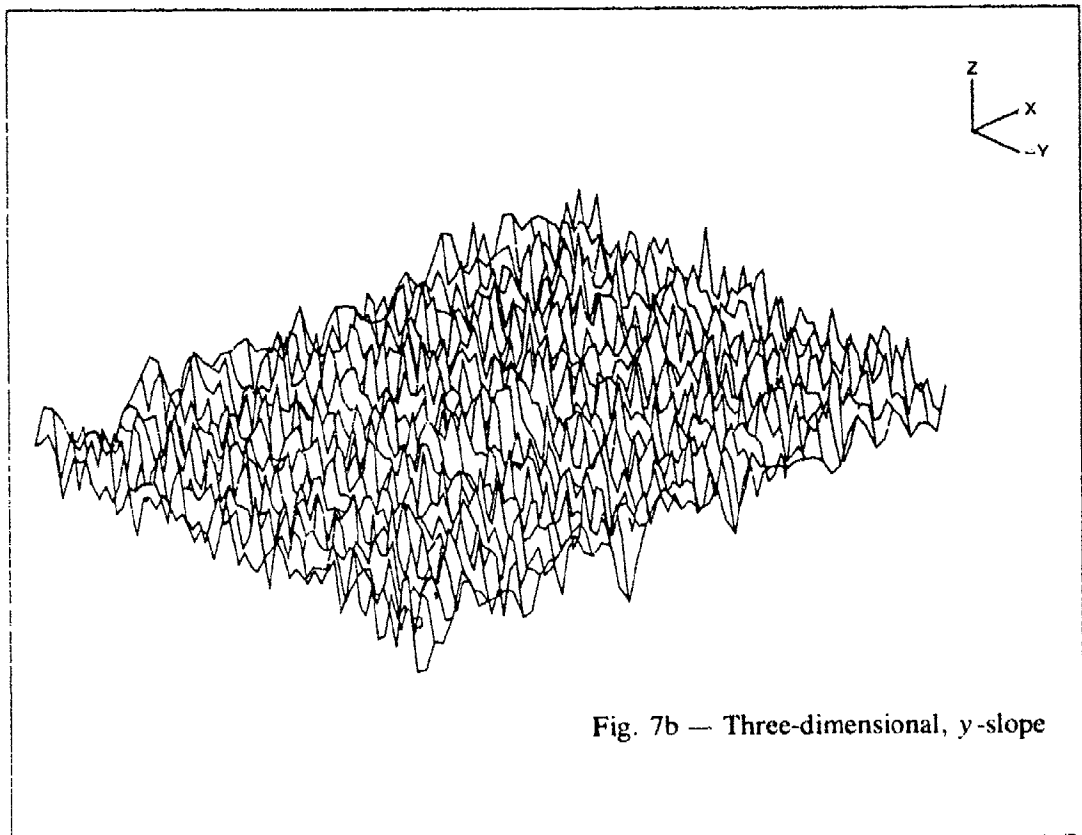
Fig. 7b — Three-dimensional, y-slope

Fig. 7 — Plots of random sea wave slopes for Sea State 5, $\beta_W = 45$ degrees
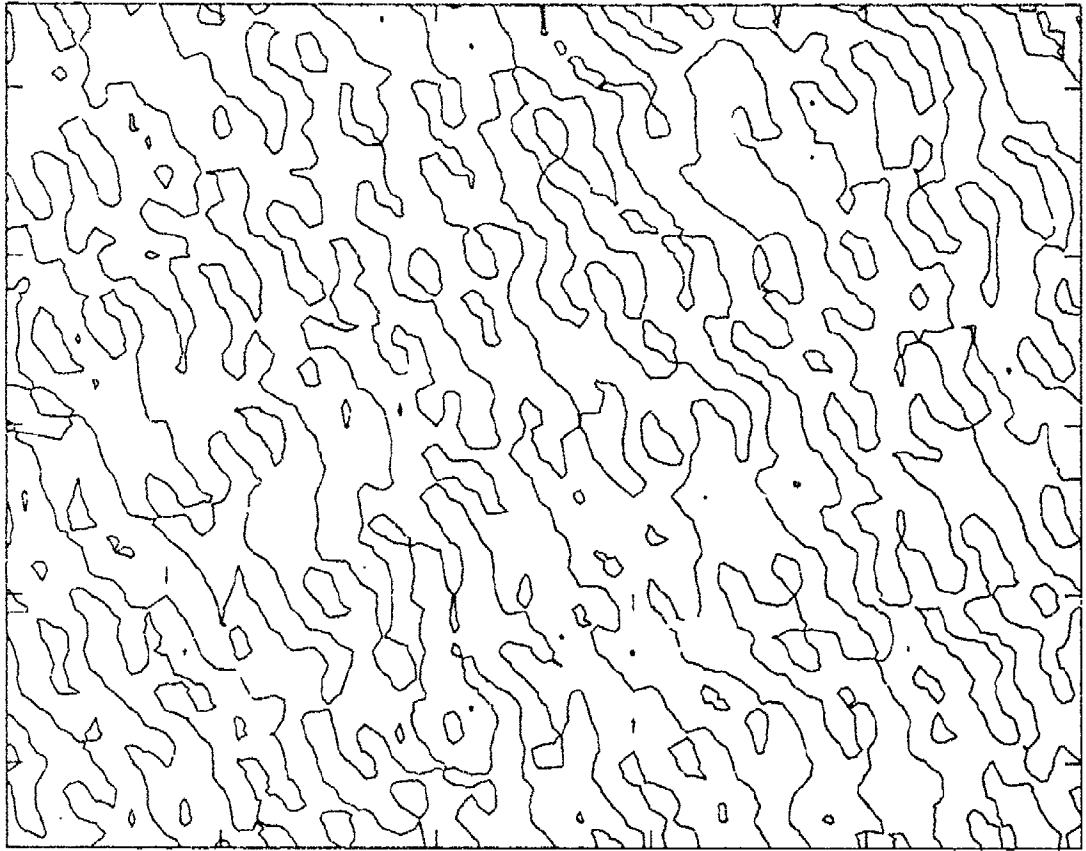
Fig. 7c — Contour, x-slope
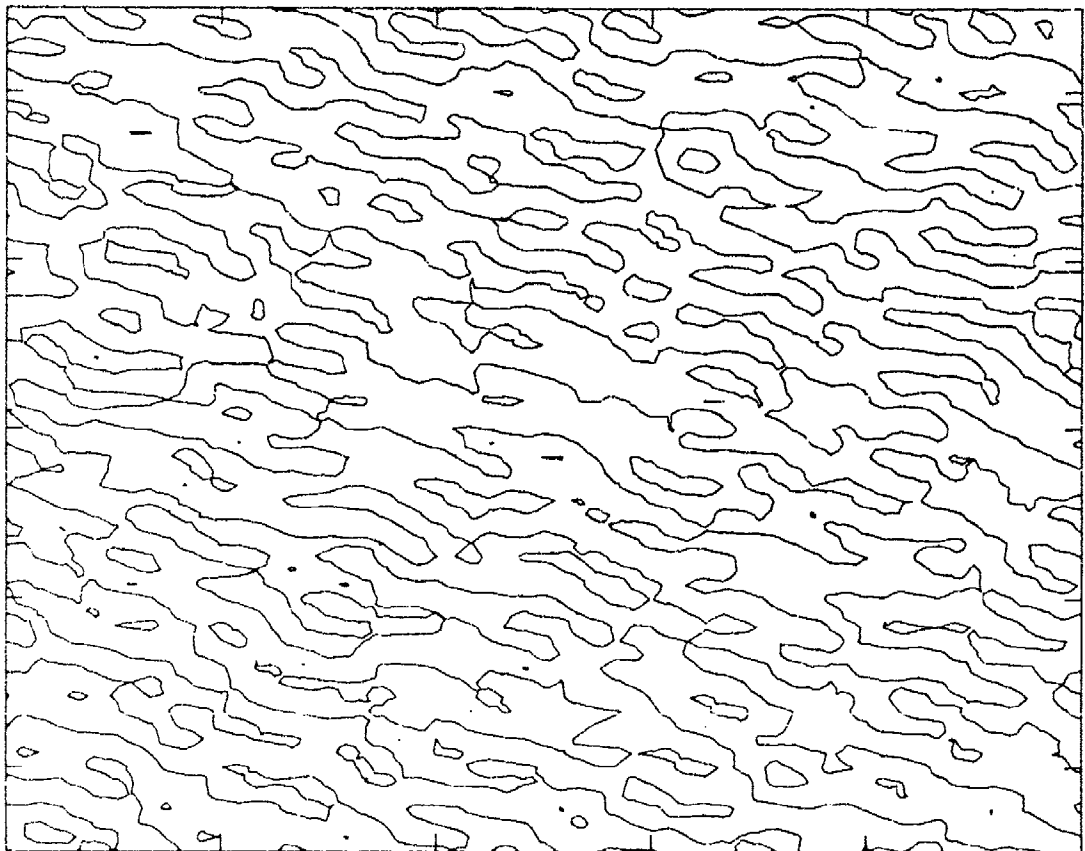
Fig. 7d –· Contour, y-slope

Fig. 7 (Continued) — Plots of random sea wave slopes for Sea State 5, $\beta_W = 45$ degrees
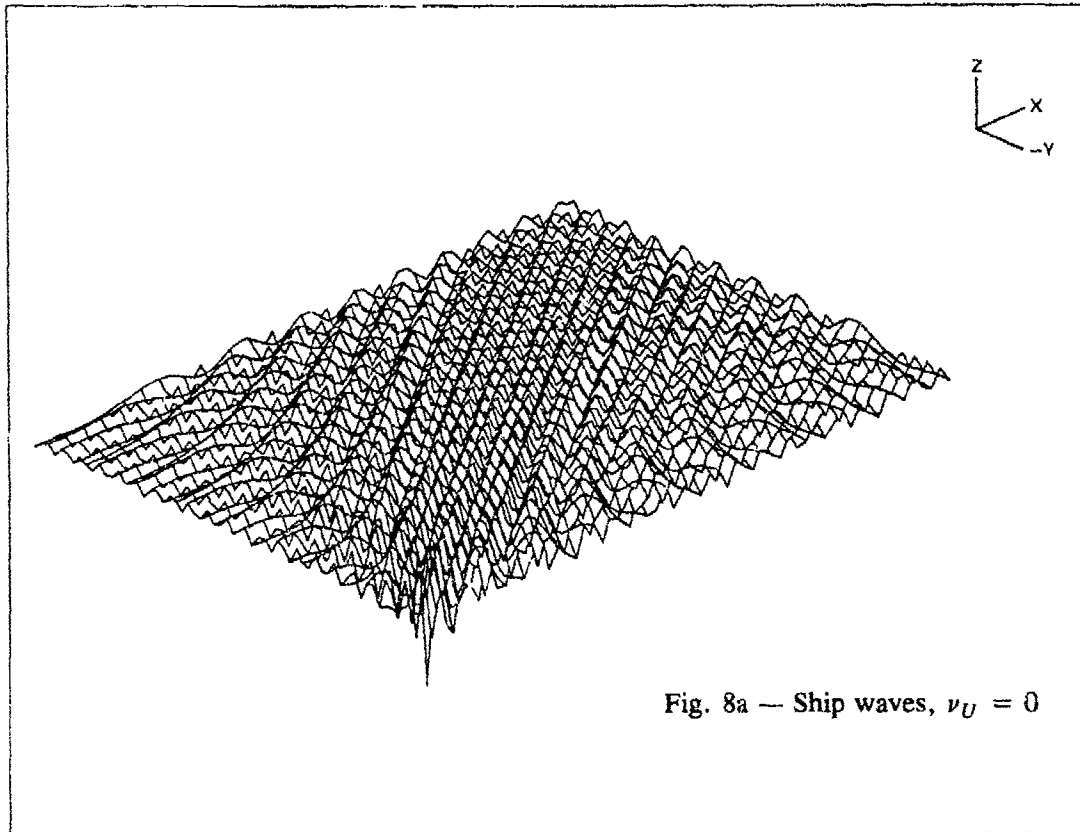
Fig. 8a — Ship waves, $\nu_U = 0$
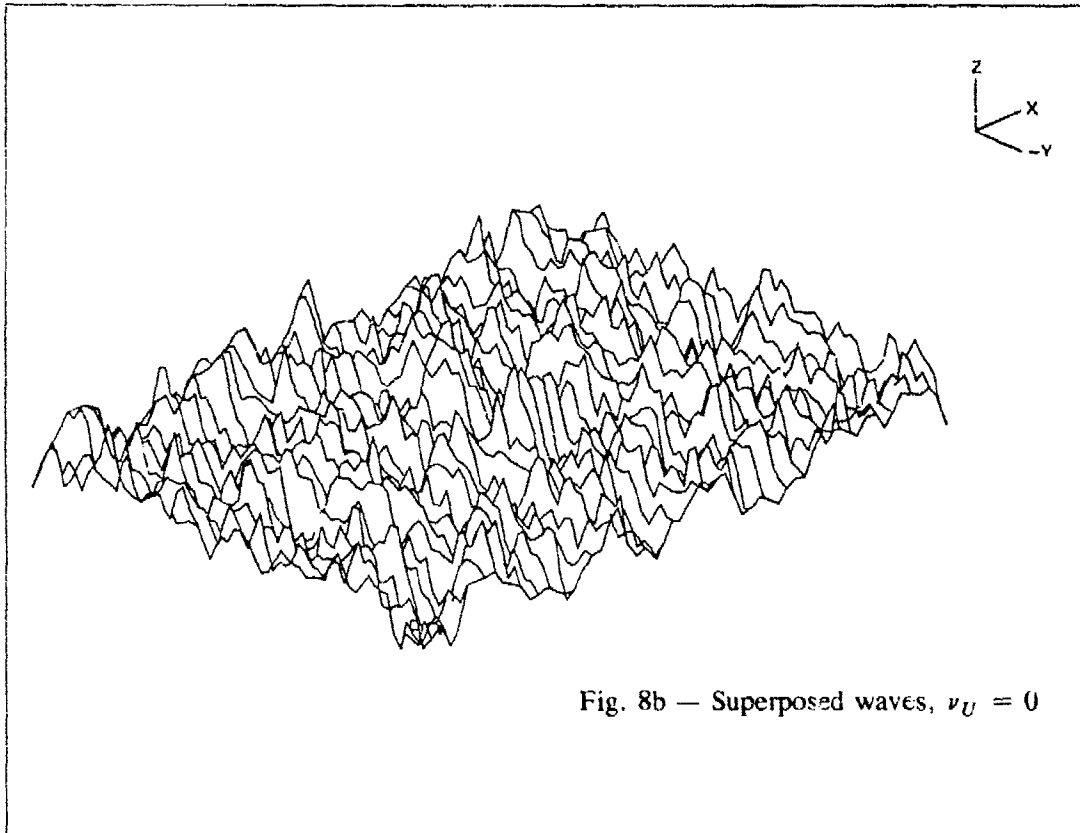
Fig. 8b — Superposed waves, $\nu_U = 0$

Fig. 8 — Three-dimensional plots of ship and superposed wave elevations for Sea State 8, $\beta_W = 45$ degrees, different values of ν_U

Fig. 8c — Ship waves, $\nu_U = 0.25$

Fig. 8d — Superposed waves, $\nu_U = 0.25$

Fig. 8 (Continued) — Three-dimensional plots of ship and superposed wave elevations for Sea State 8, $\beta_W = 45$ degrees, different values of ν_U

29

Fig. 8e — Ship waves, $\nu_U = 0.45$

Fig. 8f — Superposed waves, $\nu_U = 0.45$

Fig. 8 (Continued) — Three-dimensional plots of ship and superposed wave elevations for Sea State 8, $\beta_W = 45$ degrees, different values of ν_U

30

Fig. 9a — $U = 0$ knots

Fig. 9b — $U = 3$ knots
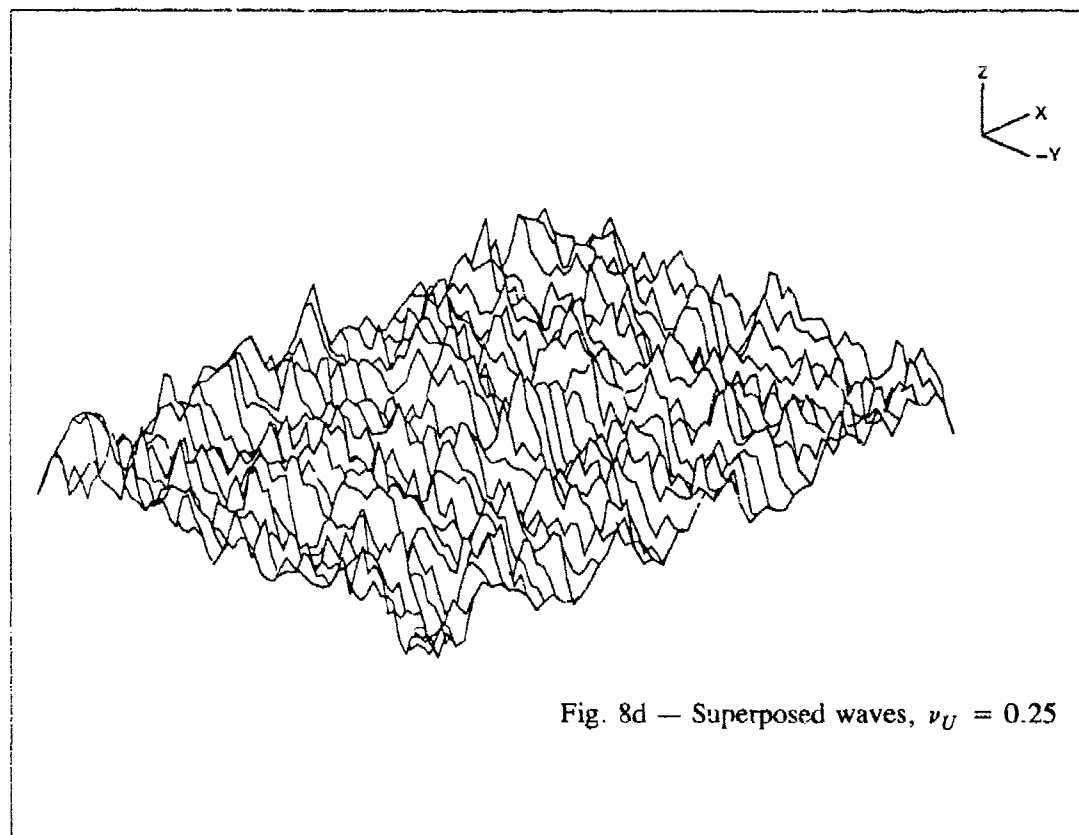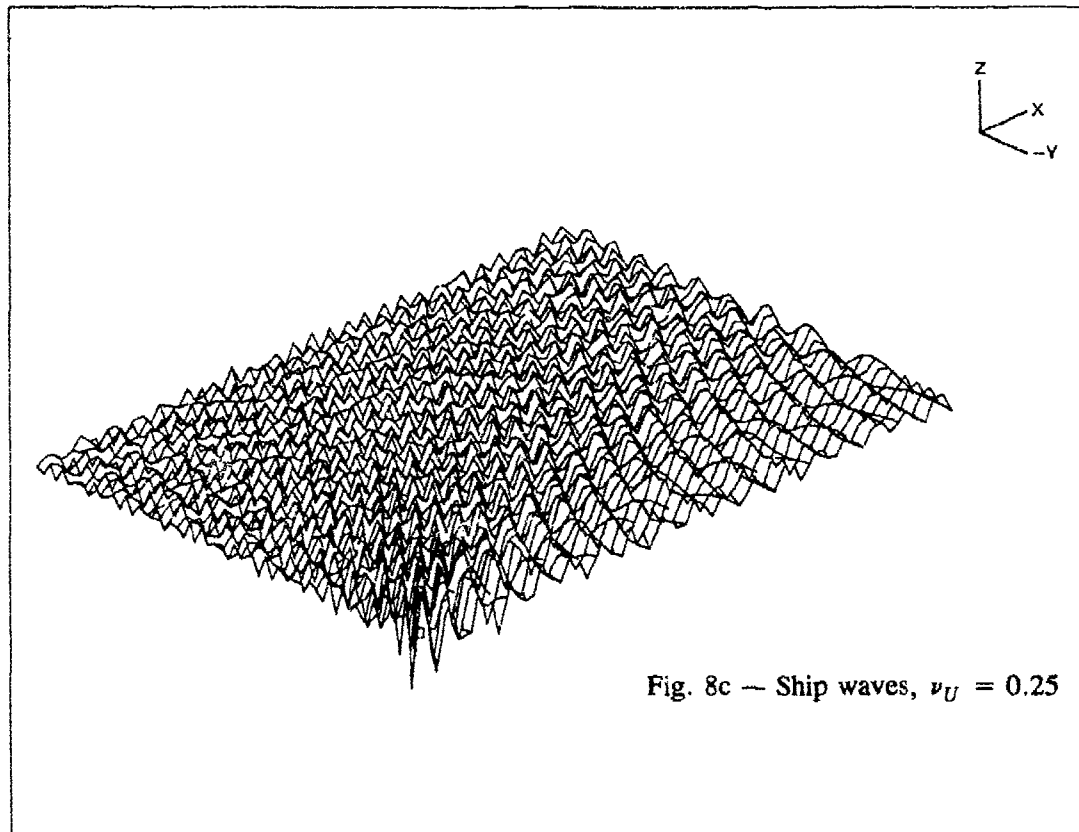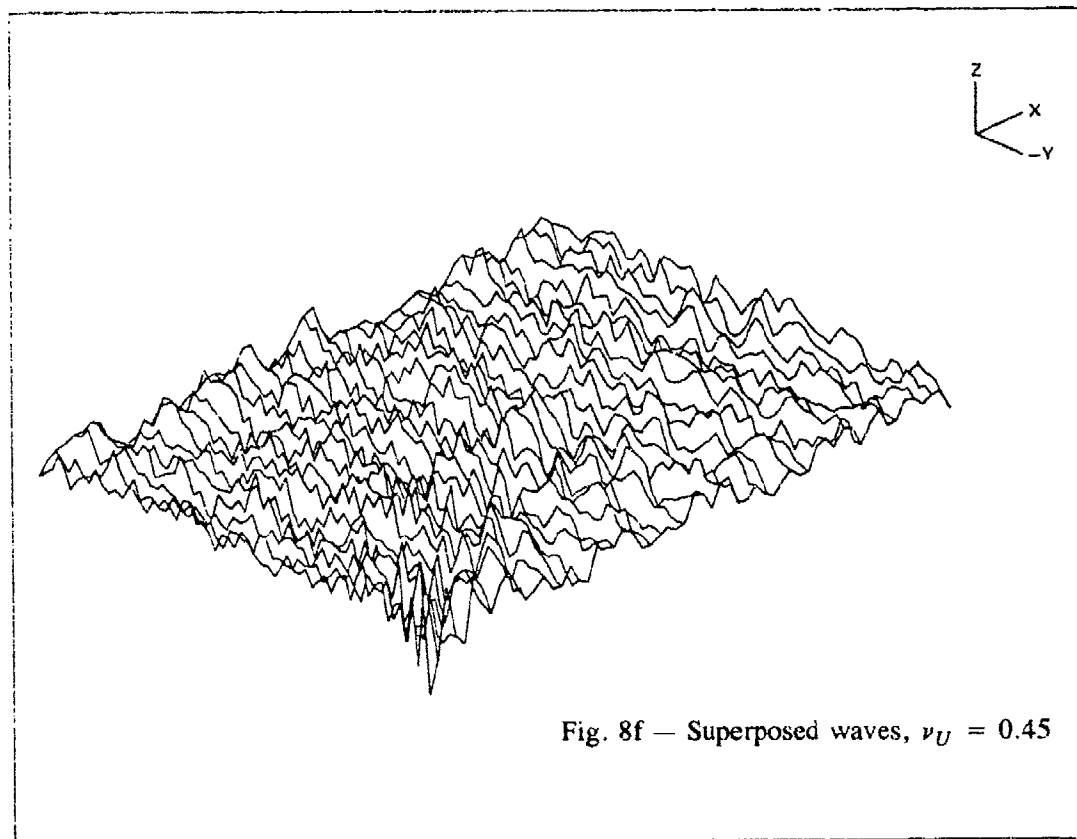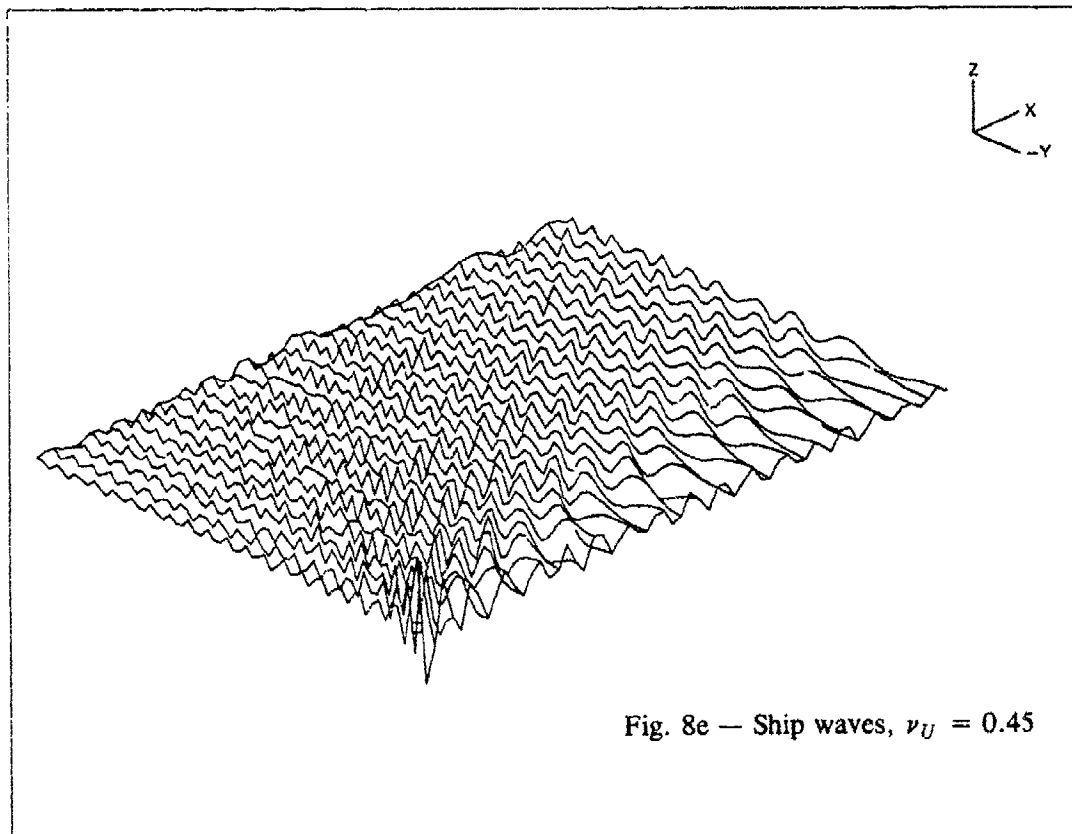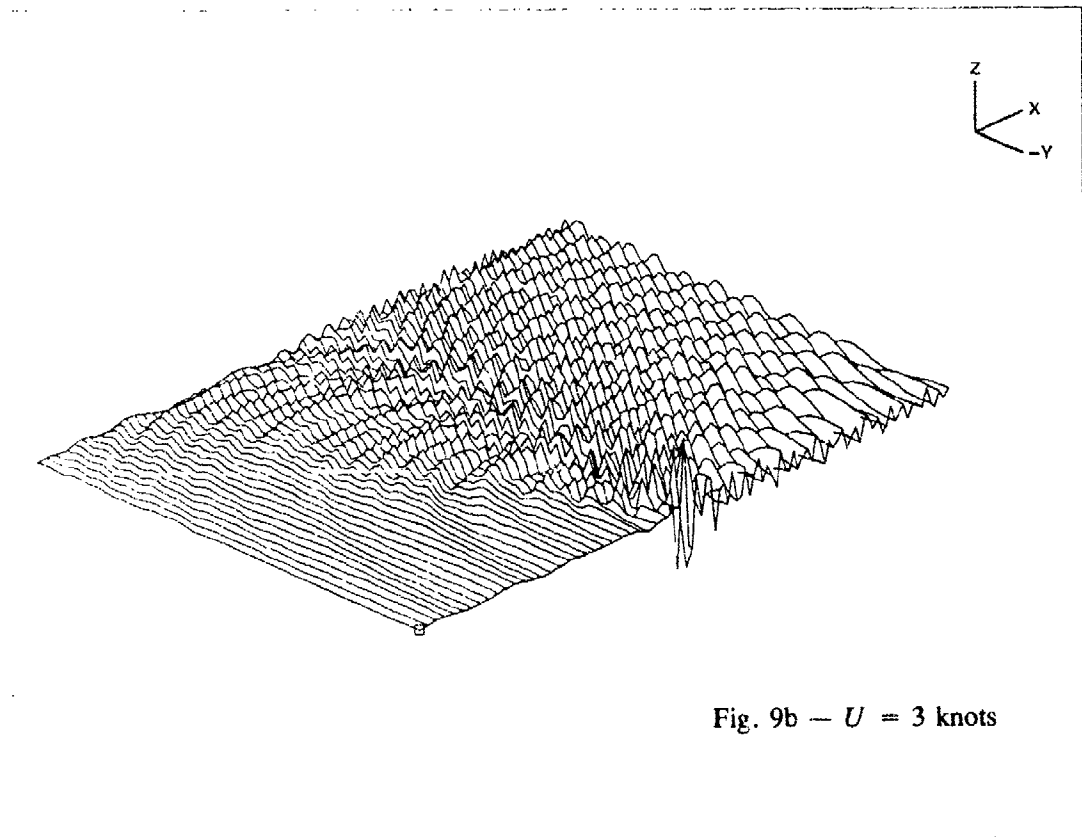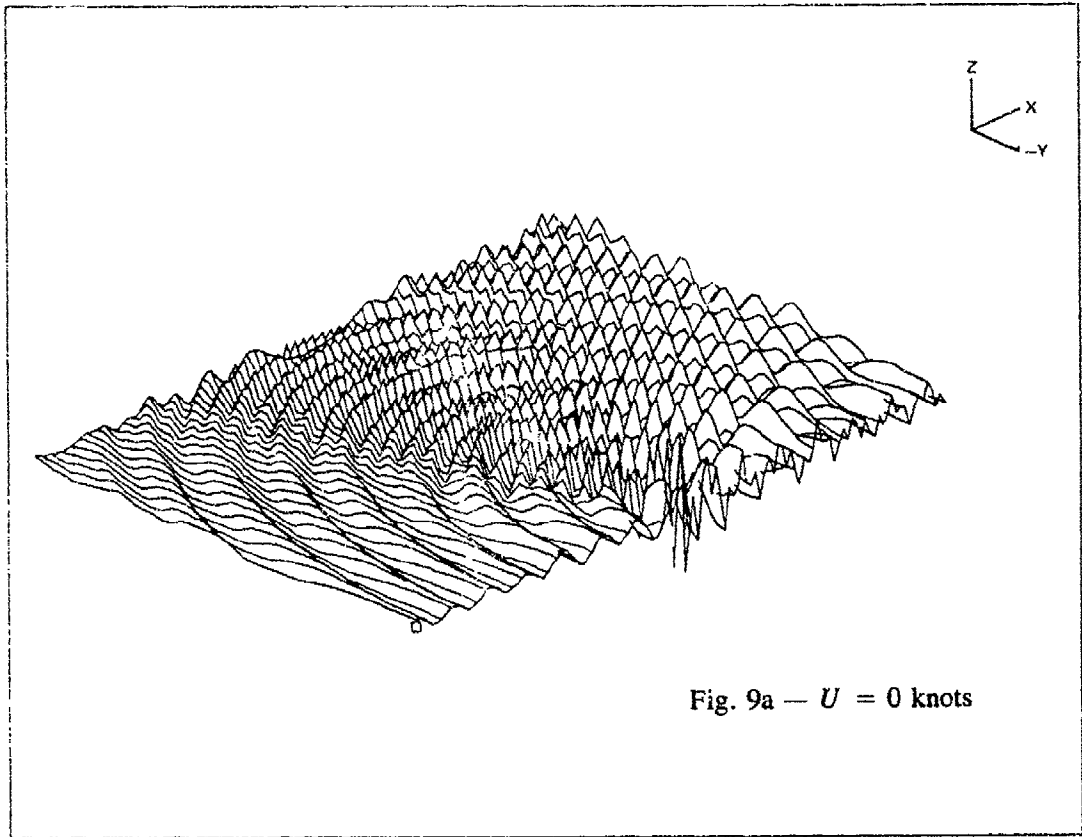
Fig. 9 — Three-dimensional plots of ship wave elevations for Sea State 5,
$\beta_W = 45$ degrees, different values of U
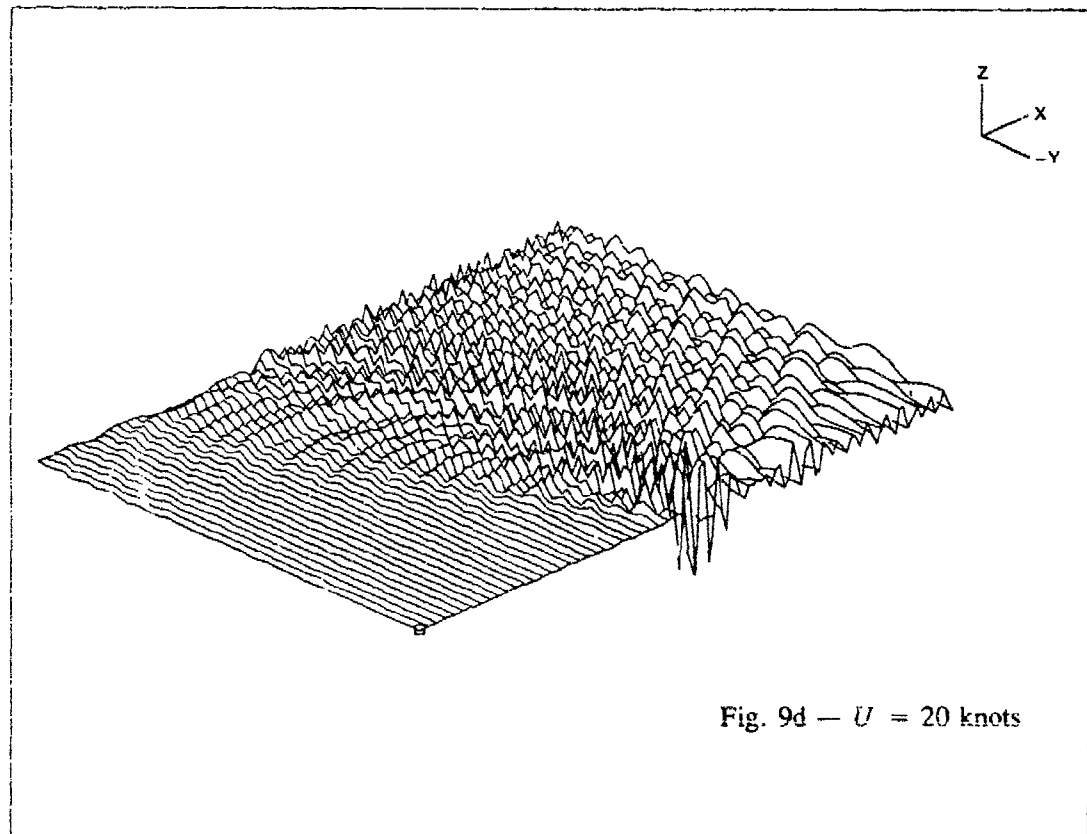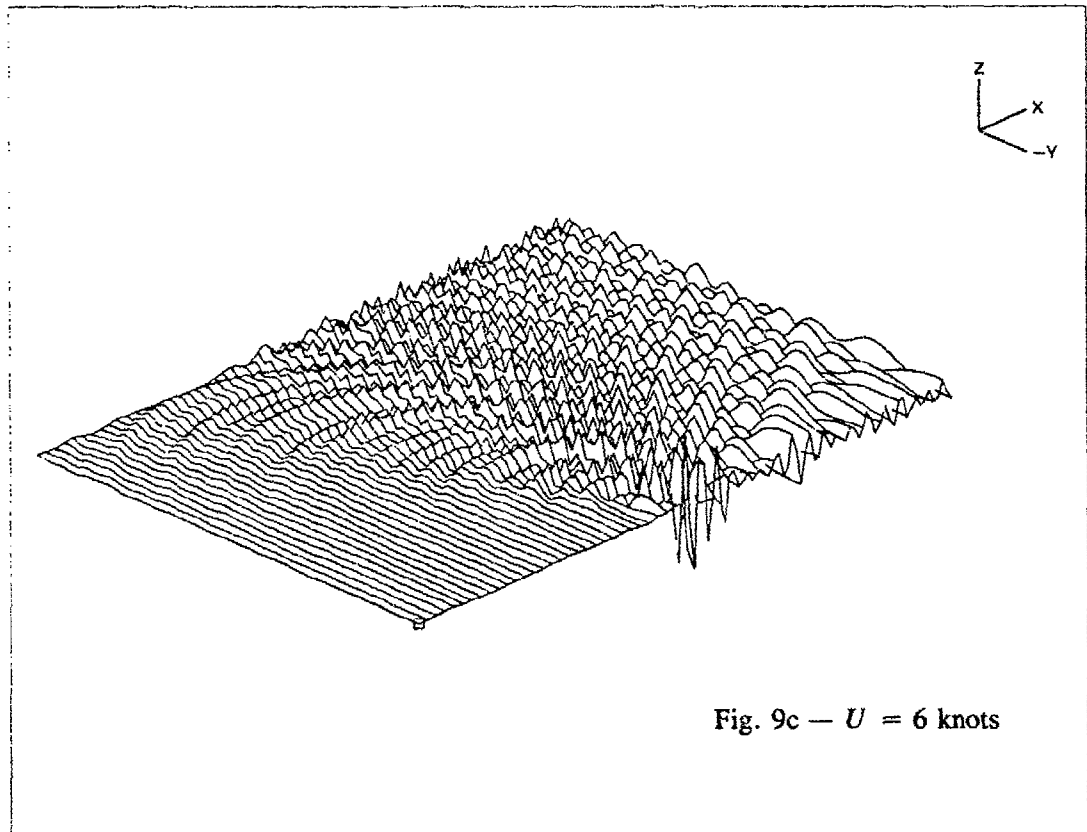
31

Fig. 9c — U = 6 knots

Fig. 9d — U = 20 knots

Fig. 9 (Continued) — Three-dimensional plots of ship wave elevations for Sea State 5, β_W = 45 degrees, different values of U

32

Fig. 10a — β_W = 45 degrees

Fig. 10b — β_W = 135 degrees
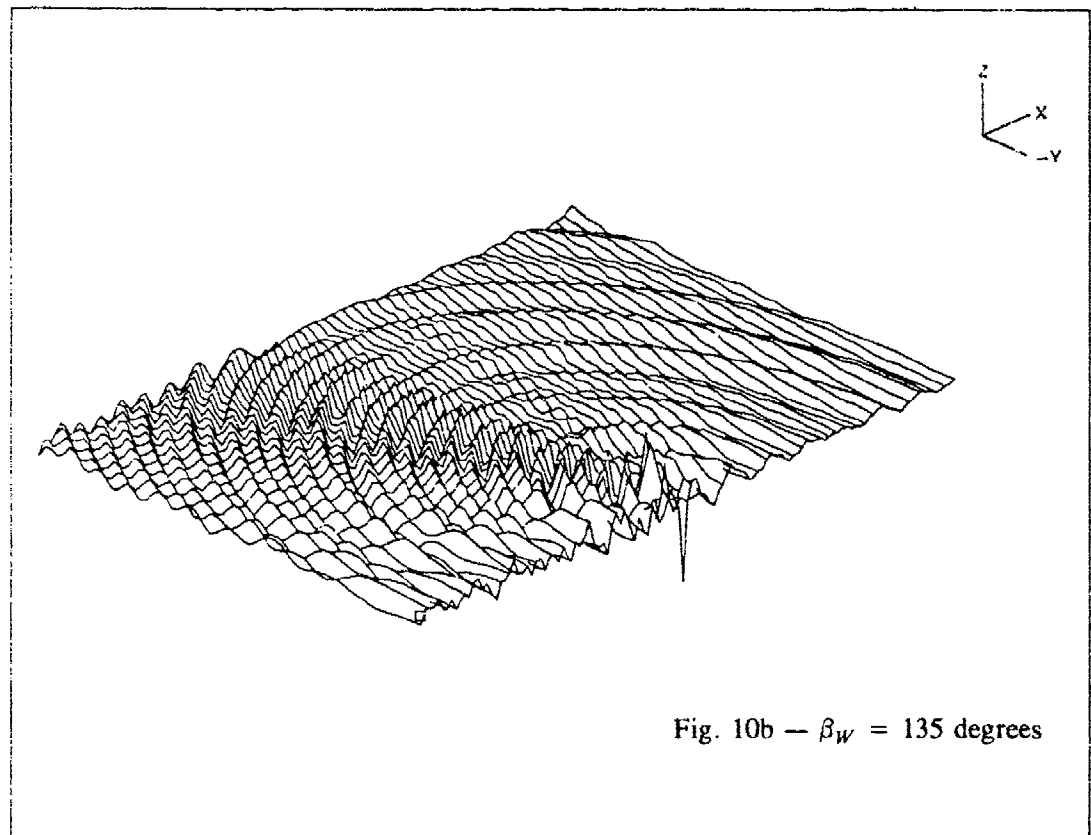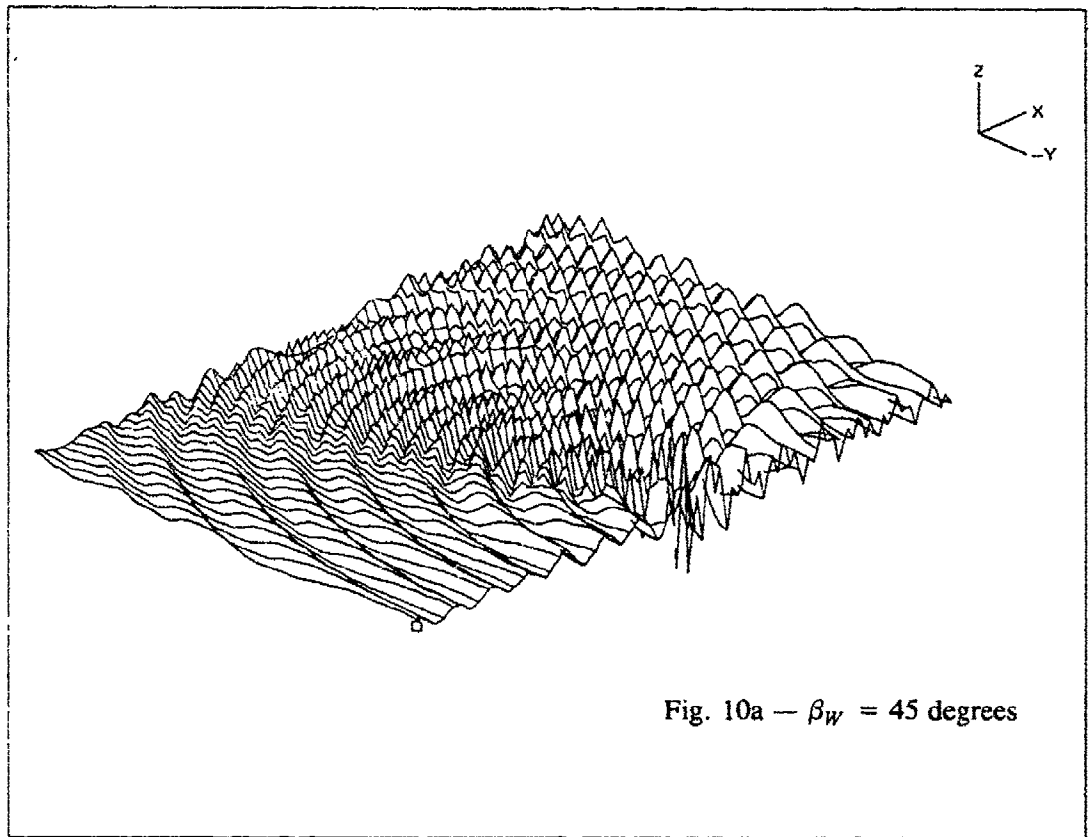
Fig. 10 — Three-dimensional plots of ship wave elevations for Sea State 5, $U = 0$, different values of β_W.

Fig. 11a — $\beta_W = 45$ degrees

Fig. 11b — $\beta_W = 135$ degrees
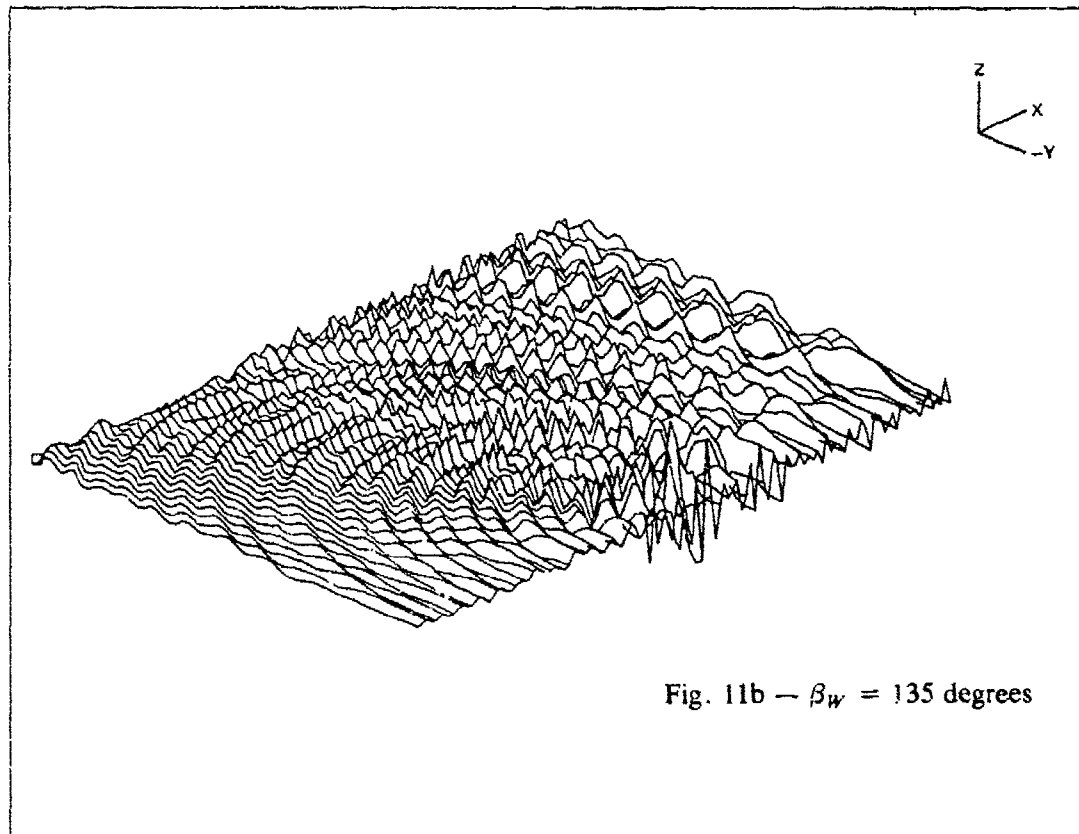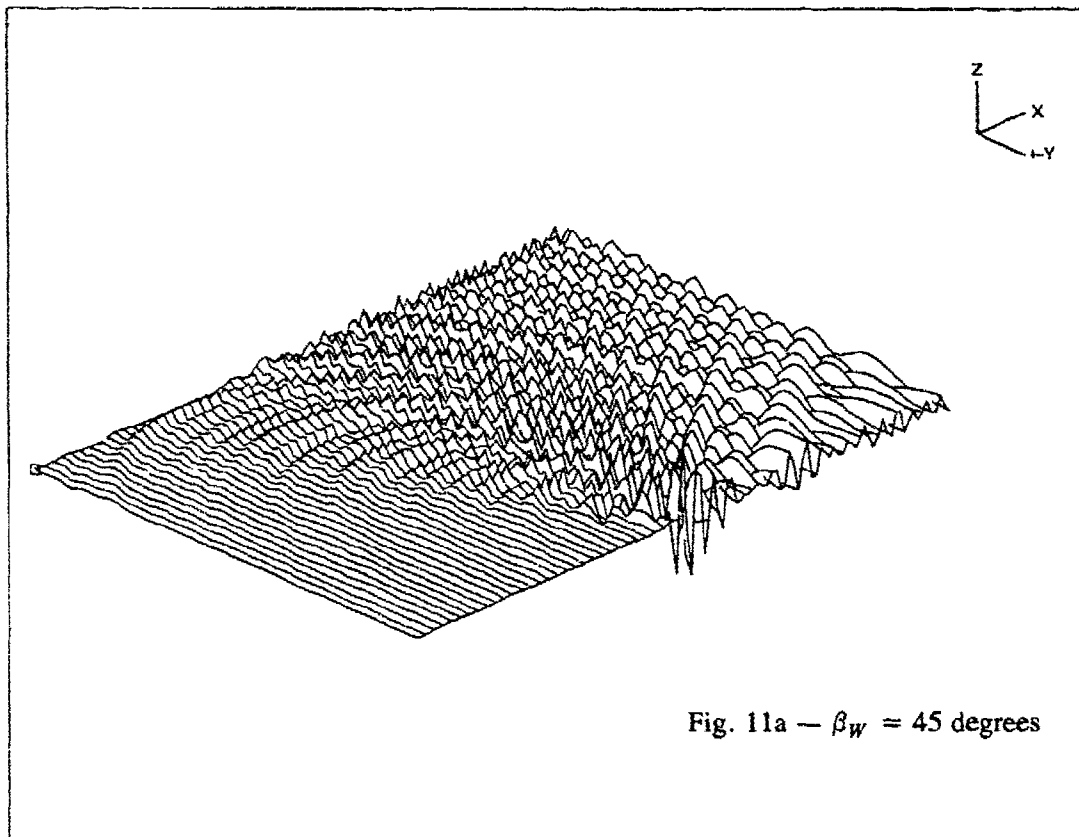
Fig. 11 — Three-dimensional plots of ship wave elevations for Sea State 5,
$U = 10$ knots, different values of β_W

Fig. 12a — Total ship waves, $U = 10$ knots

Fig. 12b — Radiation waves, $U = 10$ knots
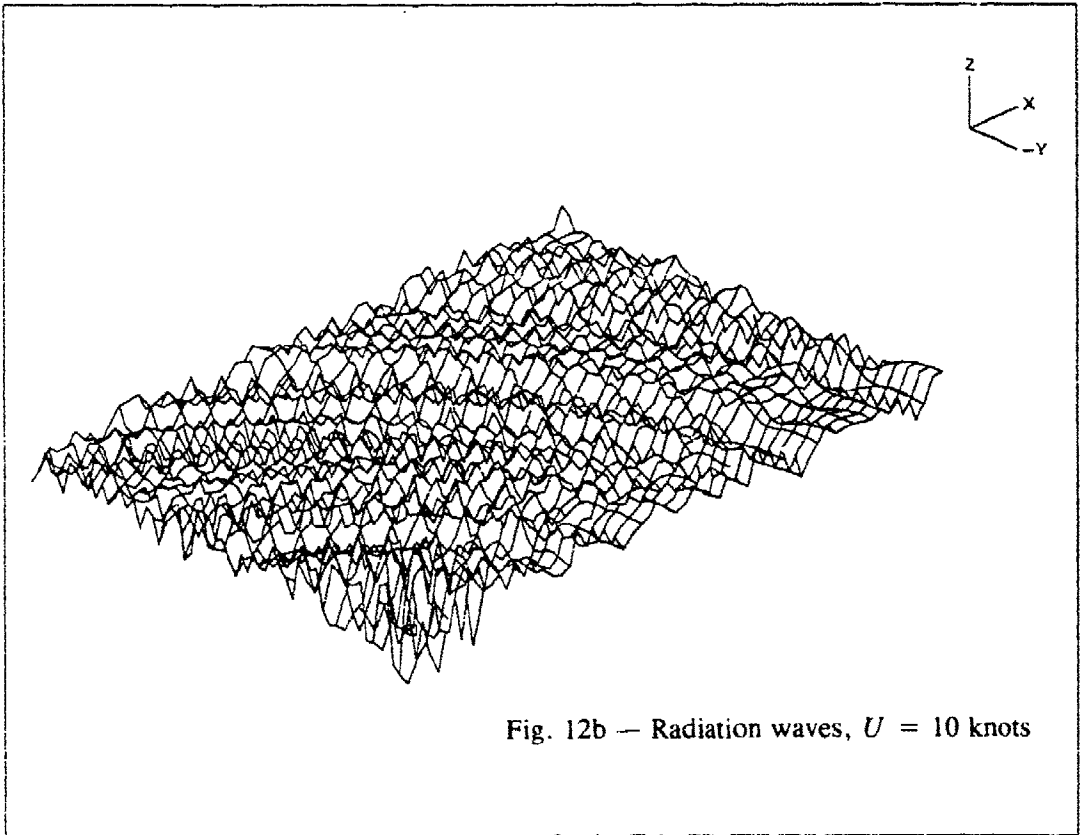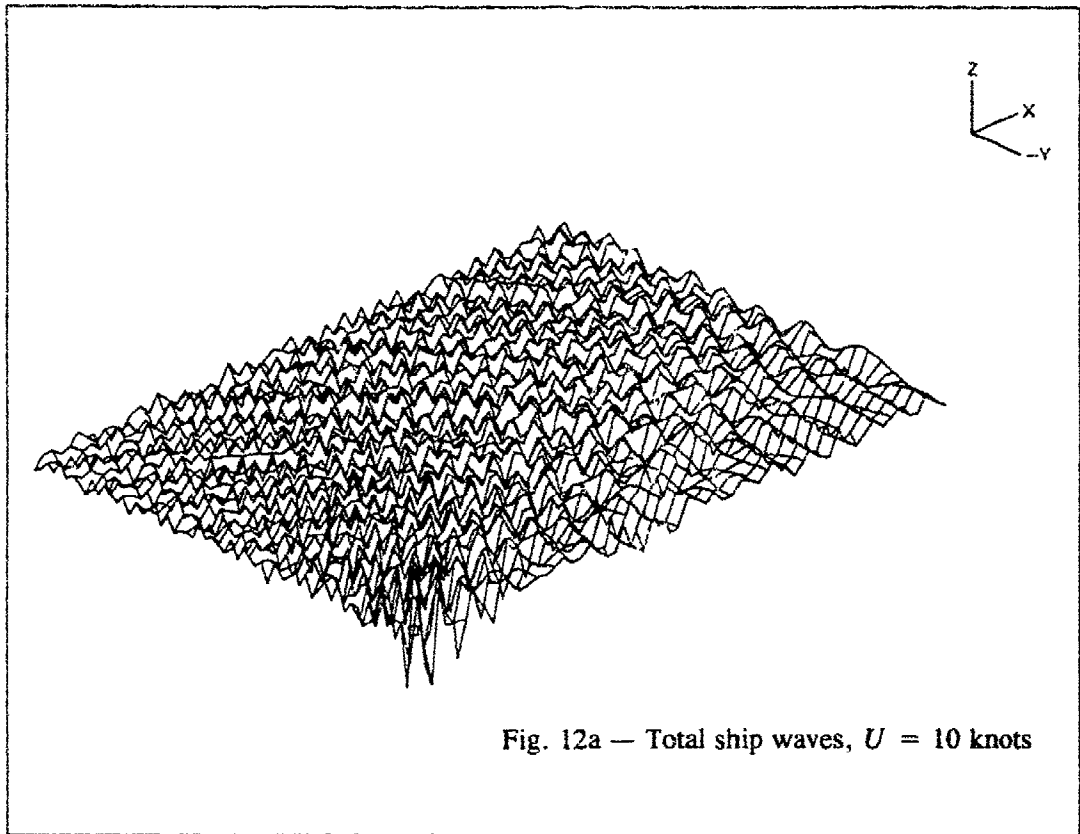
Fig. 12 — Three-dimensional plots of total ship and component radiation and diffraction wave elevations for Sea State 5, $\beta_W = 45$ degrees

Fig. 12c — Diffraction waves, U = 10 knots

Fig. 12 (Continued) — Three-dimensional plots of total ship and component radiation and diffraction wave elevations for Sea State 5, β_W = 45 degrees
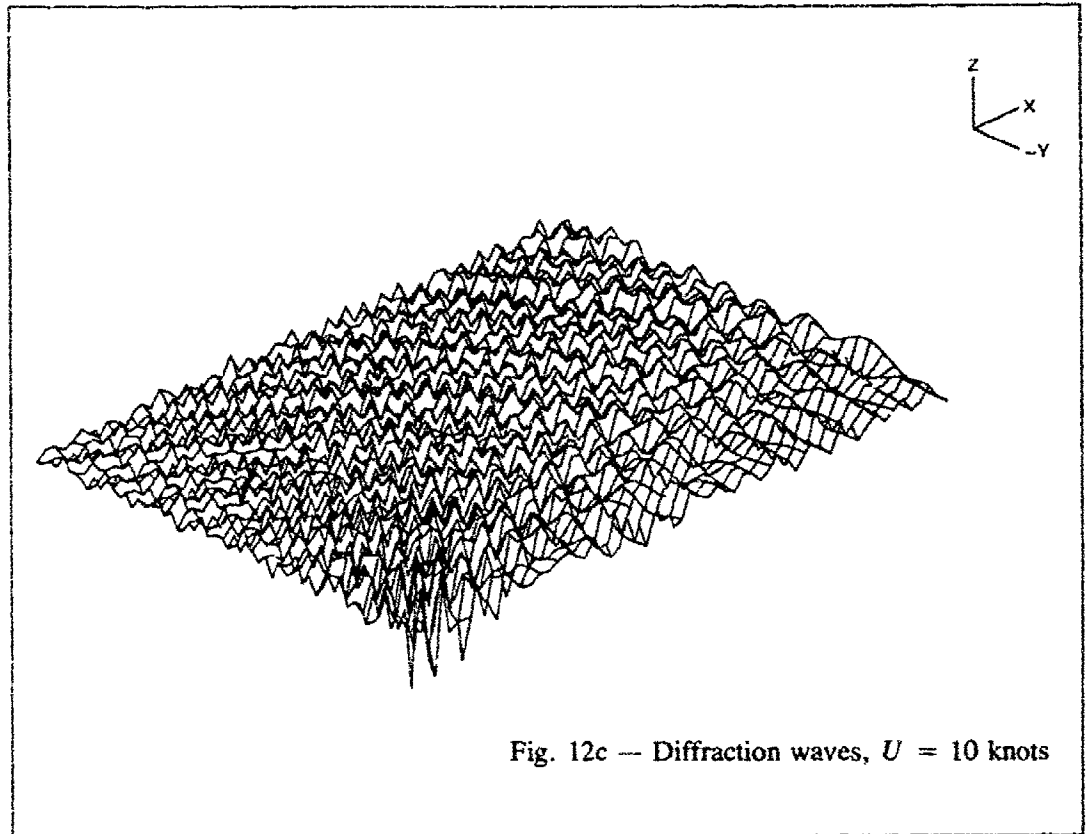
Fig. 13a — Sea State 2, U = 0 knots

Fig. 13 — Three-dimensional plots of superposed wave elevations, β_W = 45 degrees
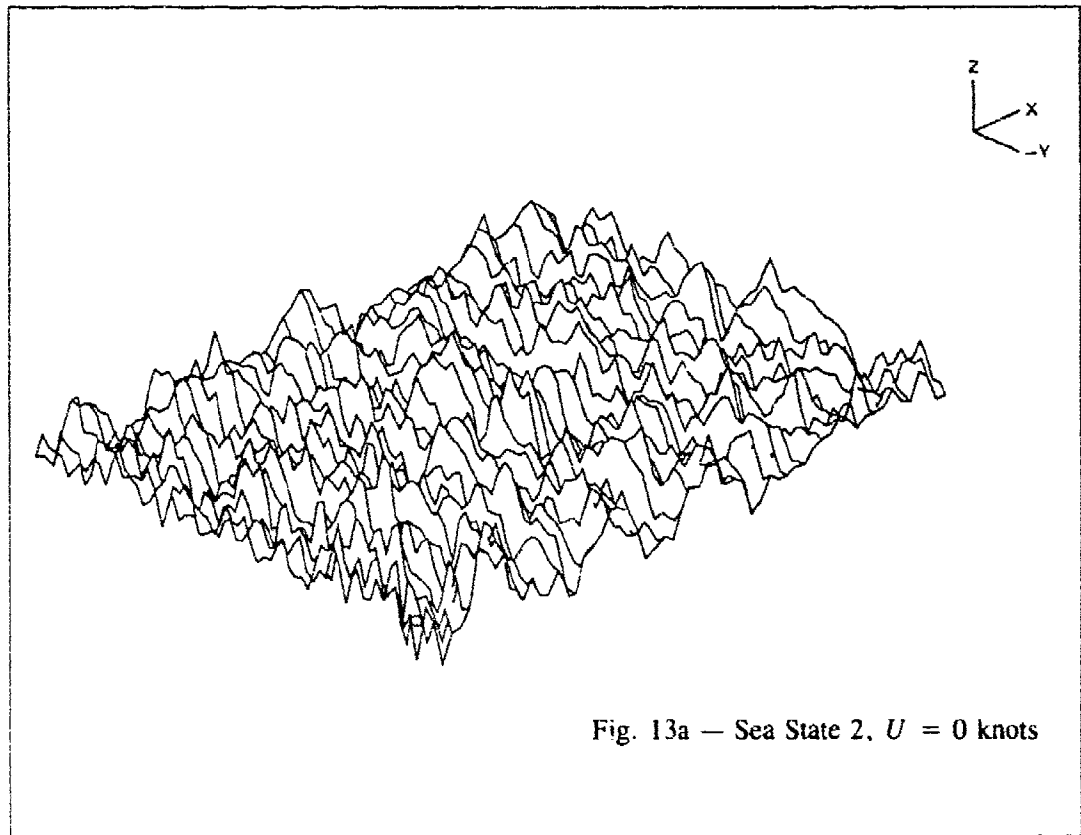
Fig. 13b — Sea State 2, U = 10 knots

Fig. 13c — Sea State 5, U = 10 knots
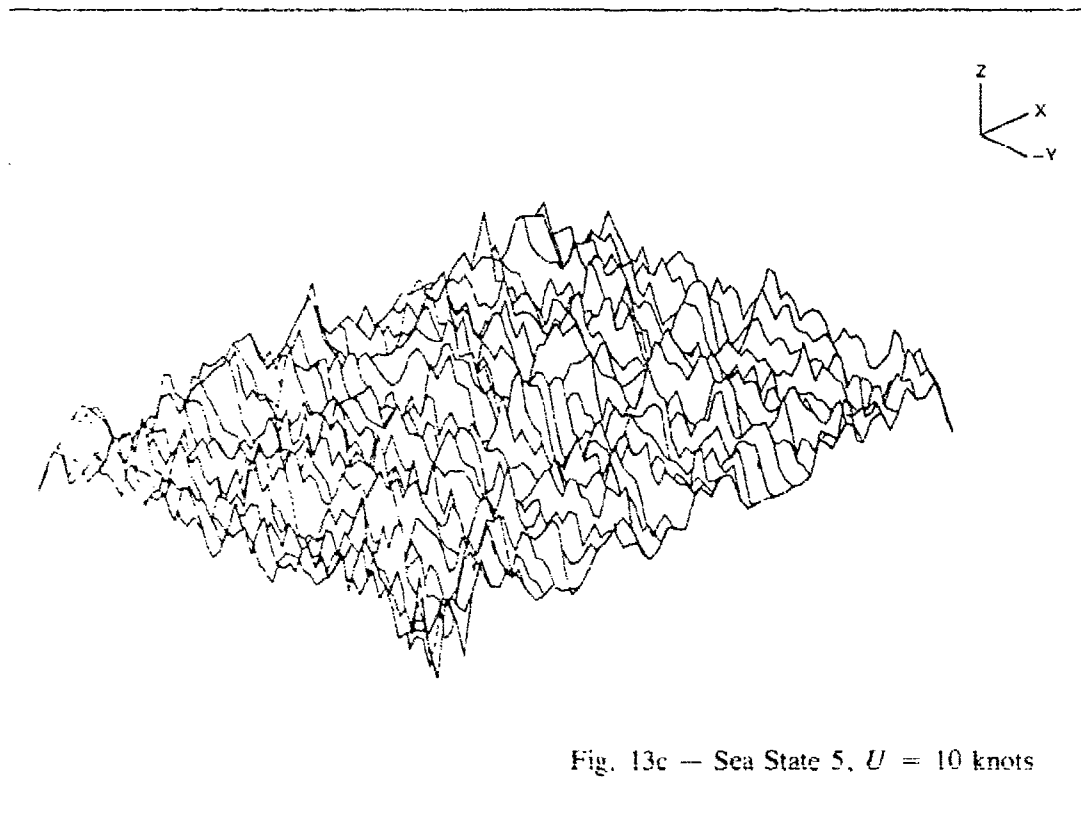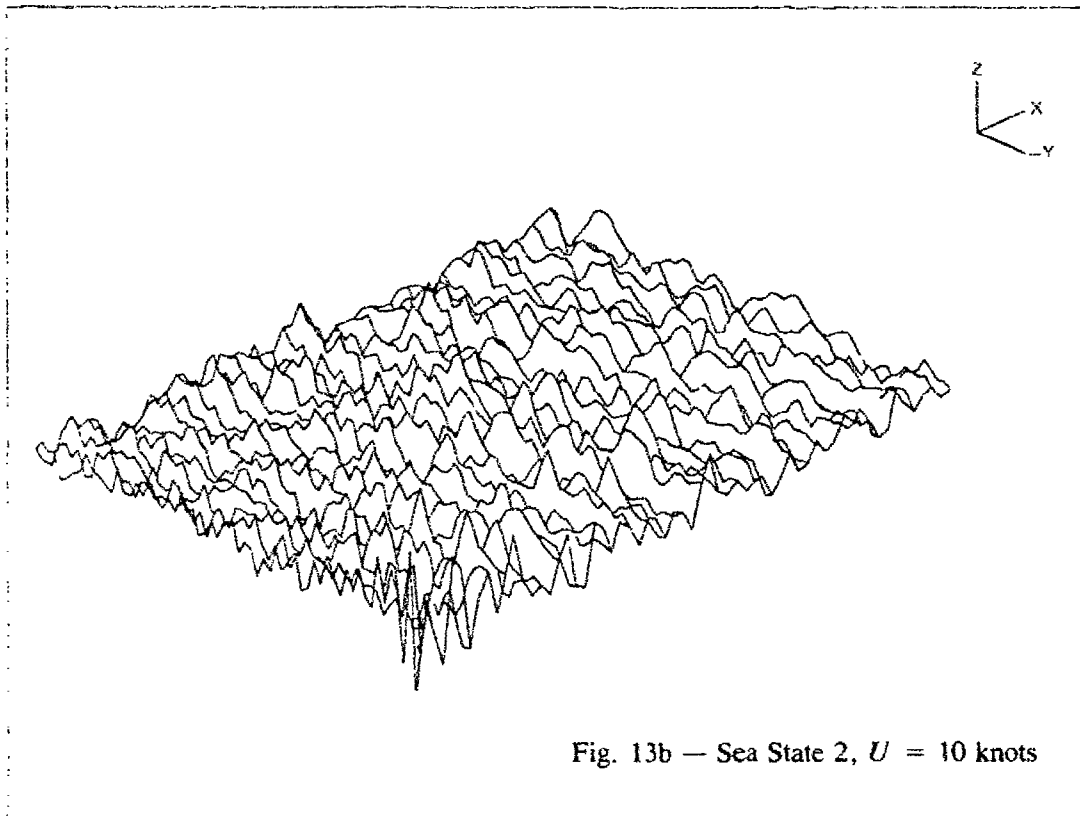
Fig. 13 (Continued) — Three-dimensional plots of superposed wave elevations, β_W = 45 degrees

37
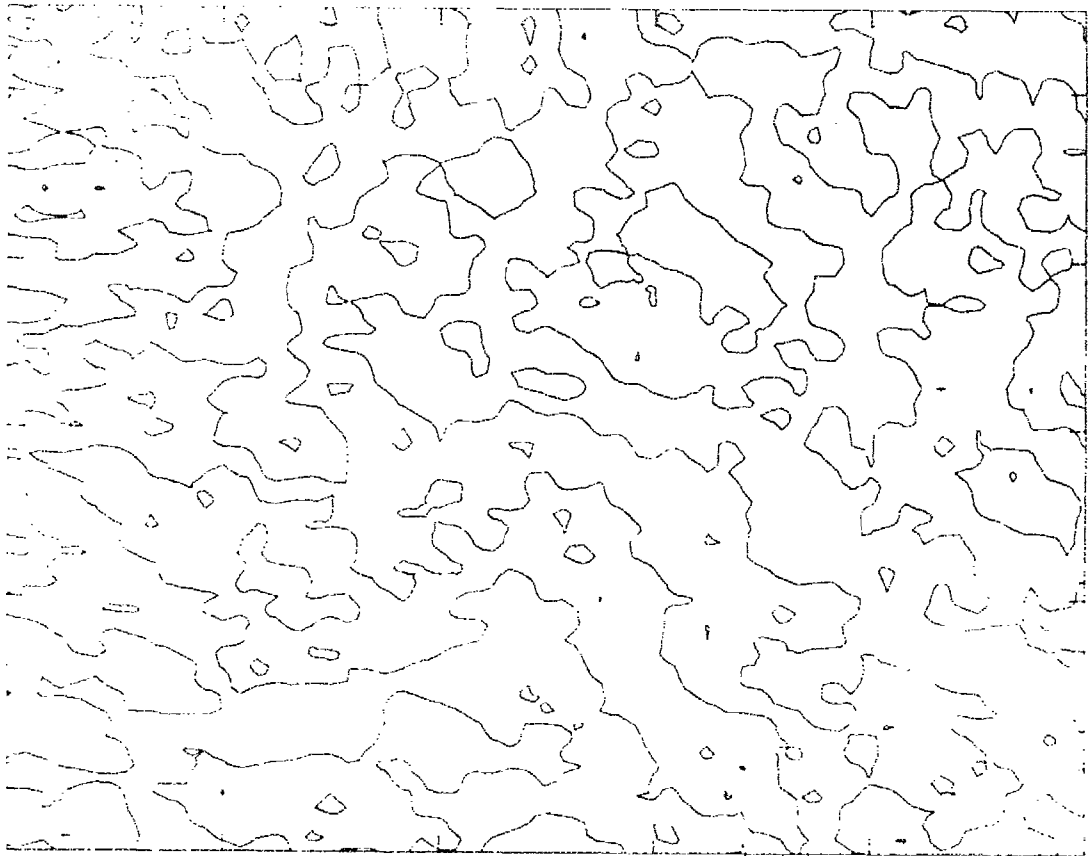
Fig. 14a — Sea State 2, $U = 0$ knots
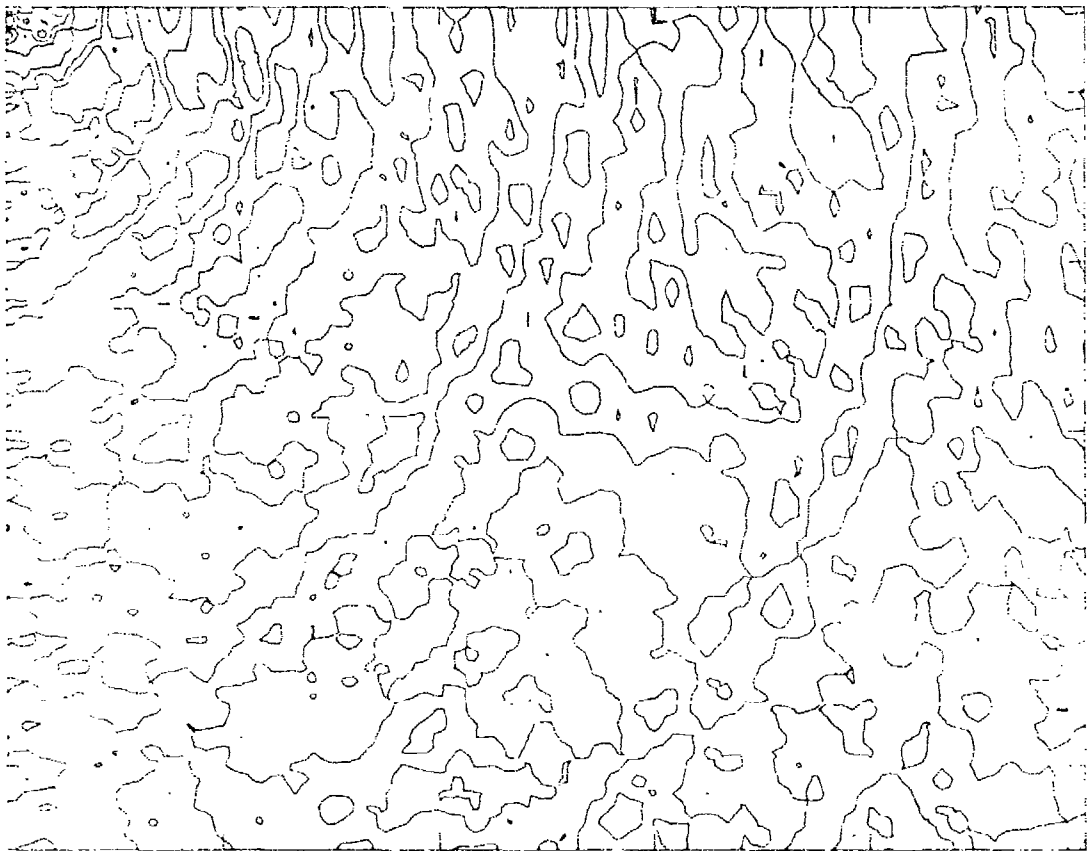
Fig. 14b — Sea State 2, $U = 10$ knots
Fig. 14 — Contour plots of superposed wave elevations, $\beta_W = 45$ degrees
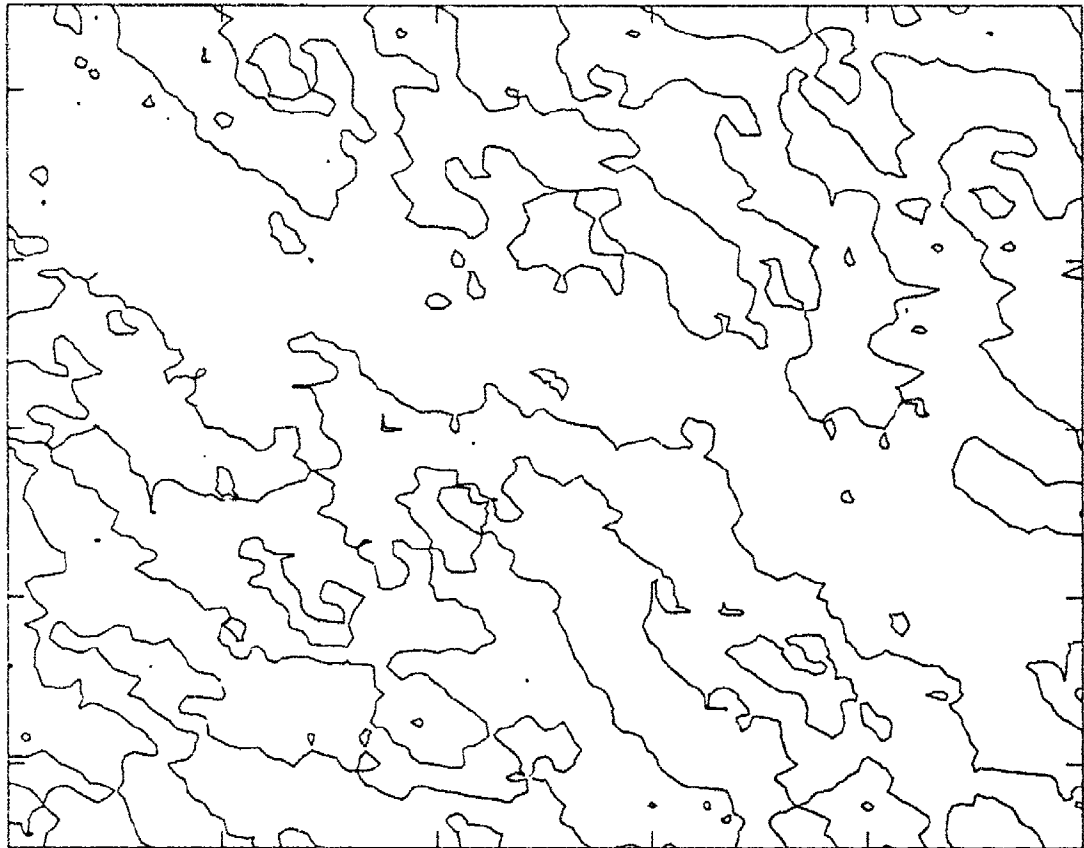
Fig. 14c — Sea State 5, $U = 10$ knots

Fig. 14 (Continued) — Contour plots of superposed wave elevations, $\beta_W = 45$ degrees
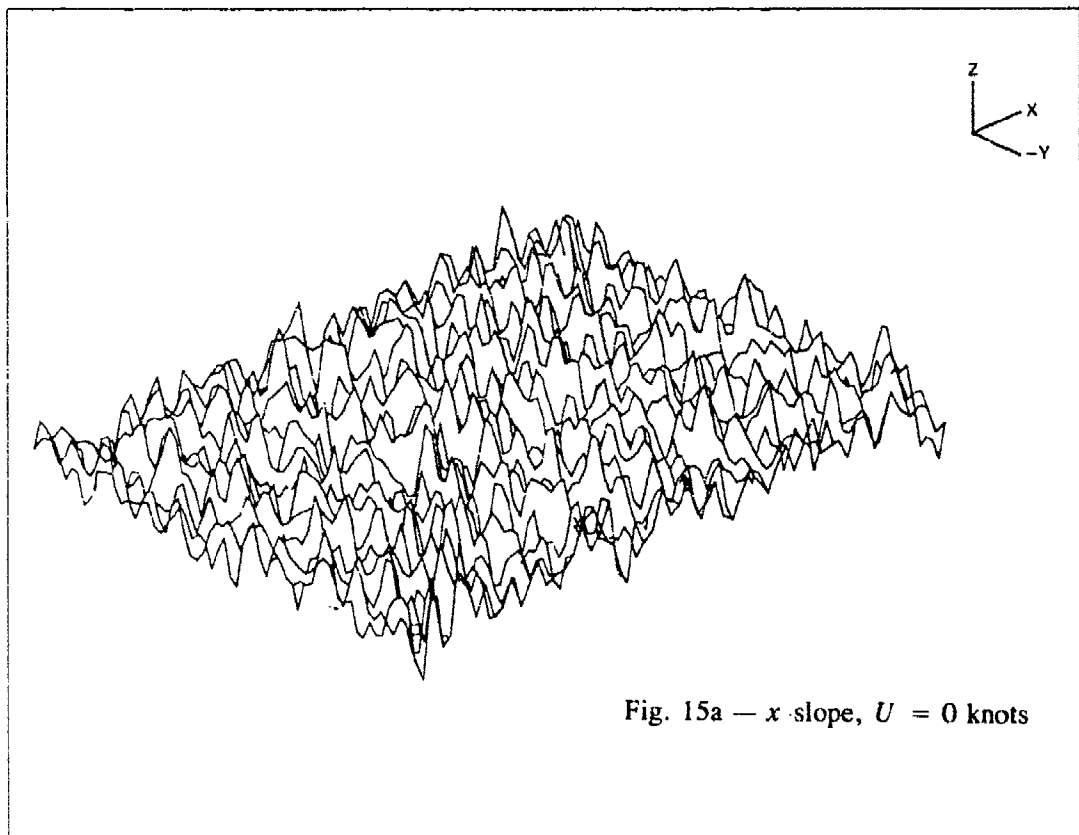
Fig. 15a — x slope, $U = 0$ knots

Fig. 15 — Three-dimensional plots of superposed wave slopes for Sea State 5, $\beta_W = 45$ degrees
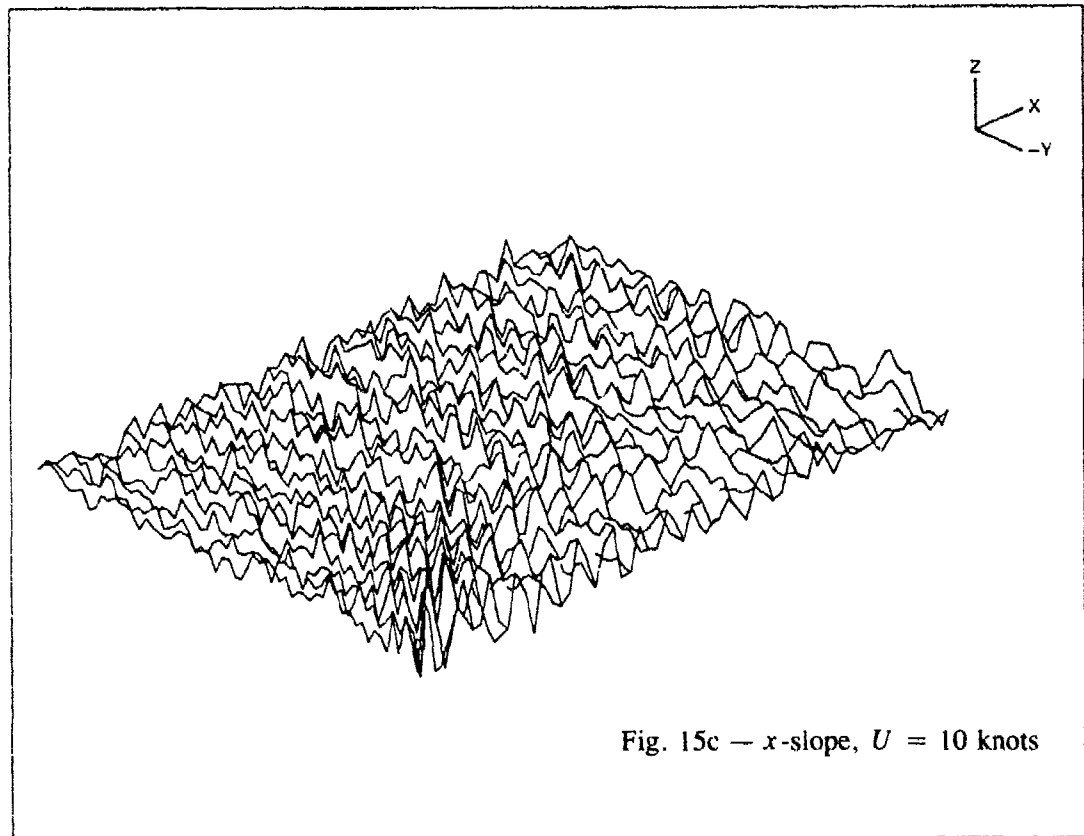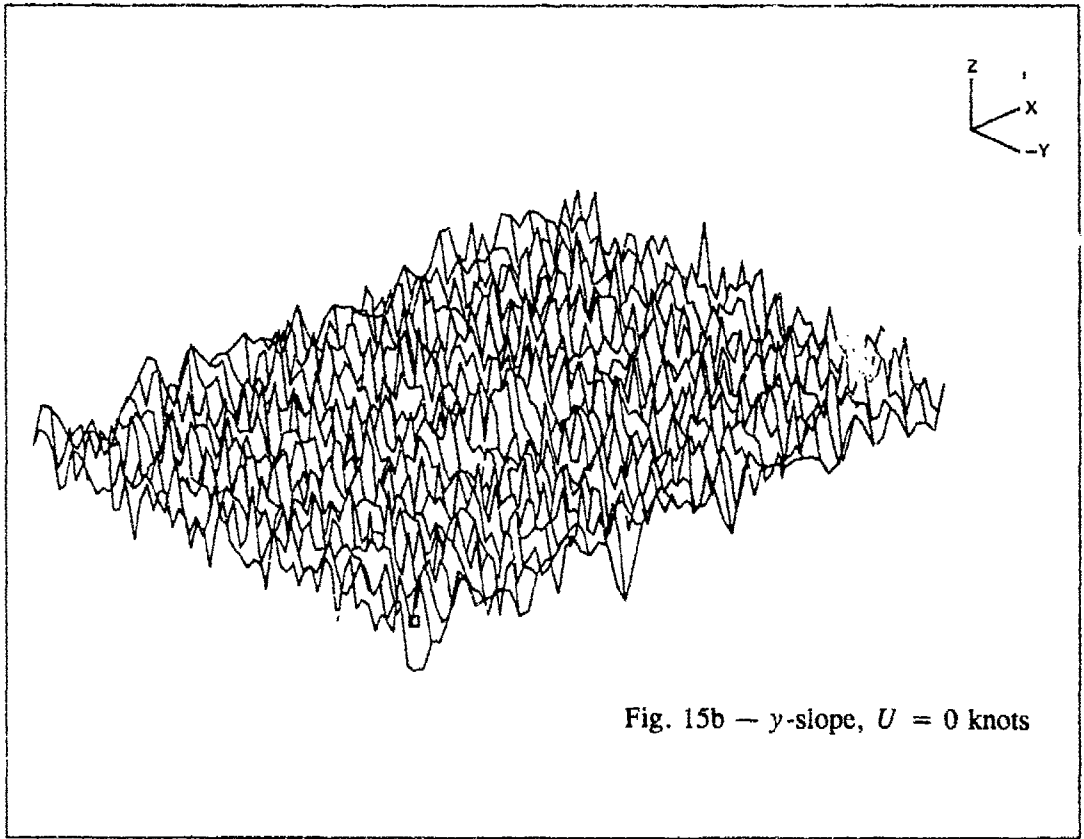
Fig. 15b — y-slope, $U = 0$ knots

Fig. 15c — x-slope, $U = 10$ knots

Fig. 15 (Continued) — Three-dimensional plots of superposed wave slopes
for Sea State 5, $\beta_W = 45$ degrees

Fig. 15d — y-slope, U = 10 knots
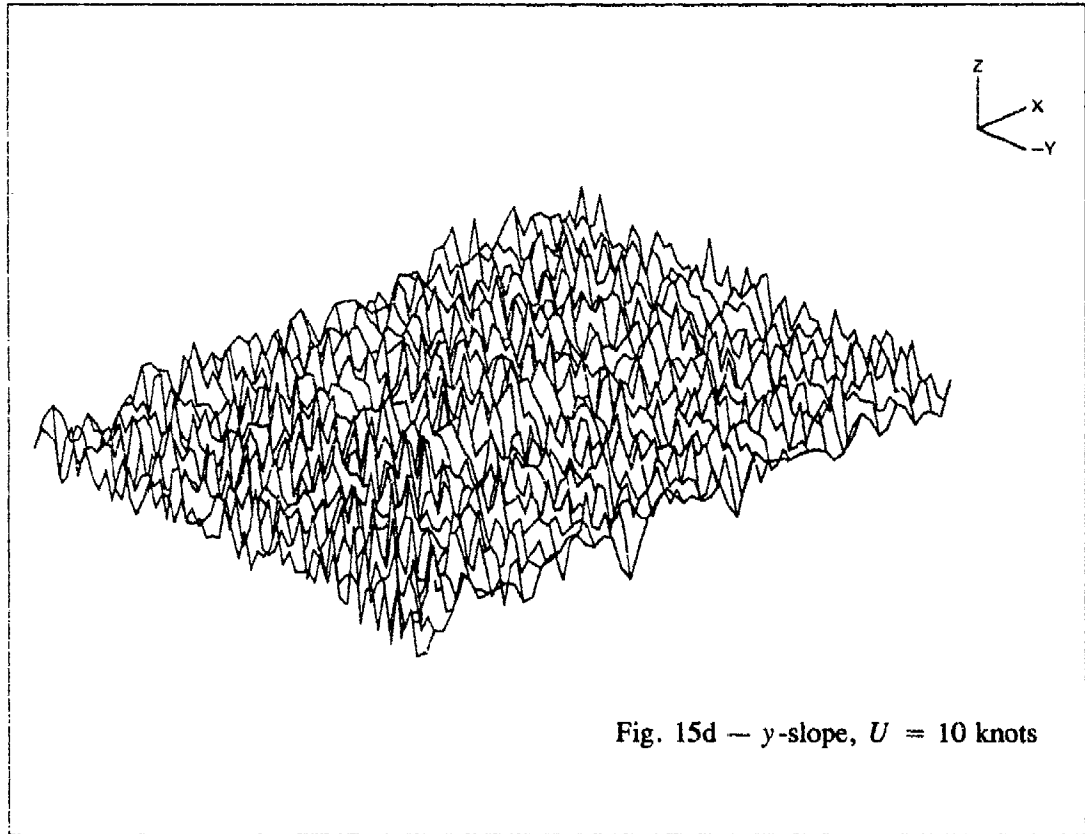
Fig. 15 (Continued) — Three-dimensional plots of superposed wave slopes
for Sea State 5, β_W = 45 degrees
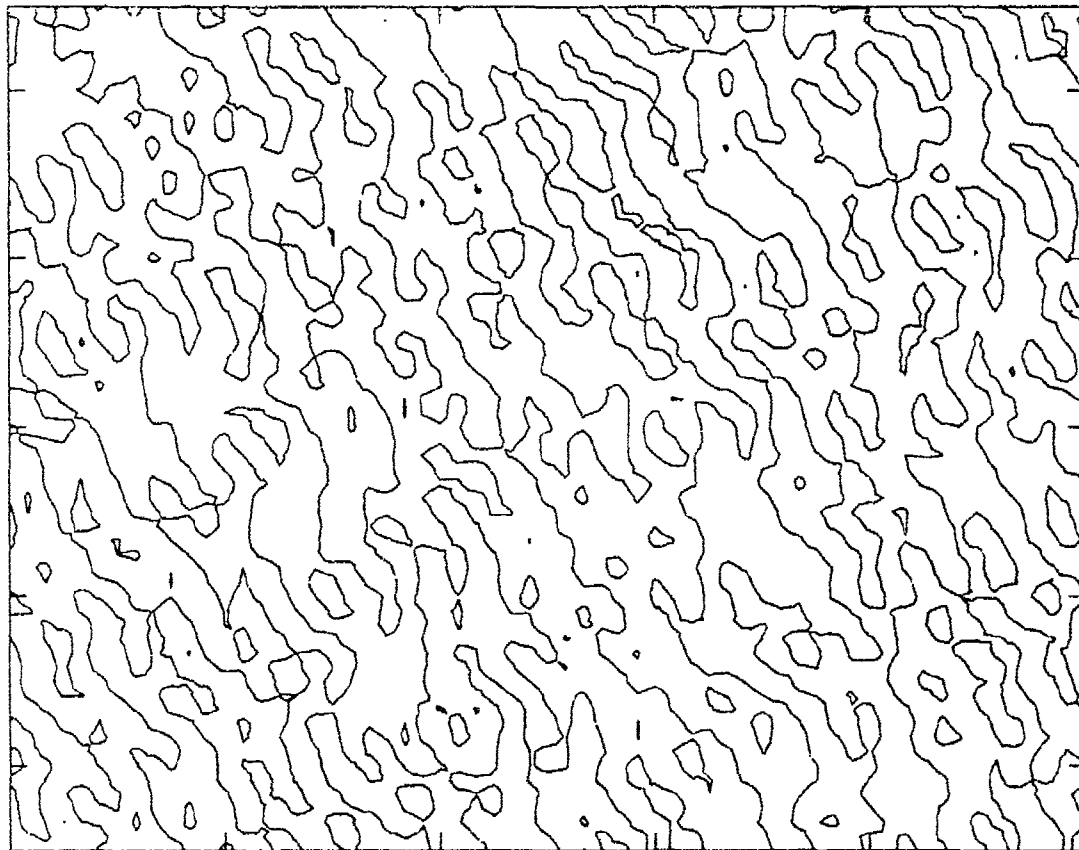
Fig. 16a — x-slope
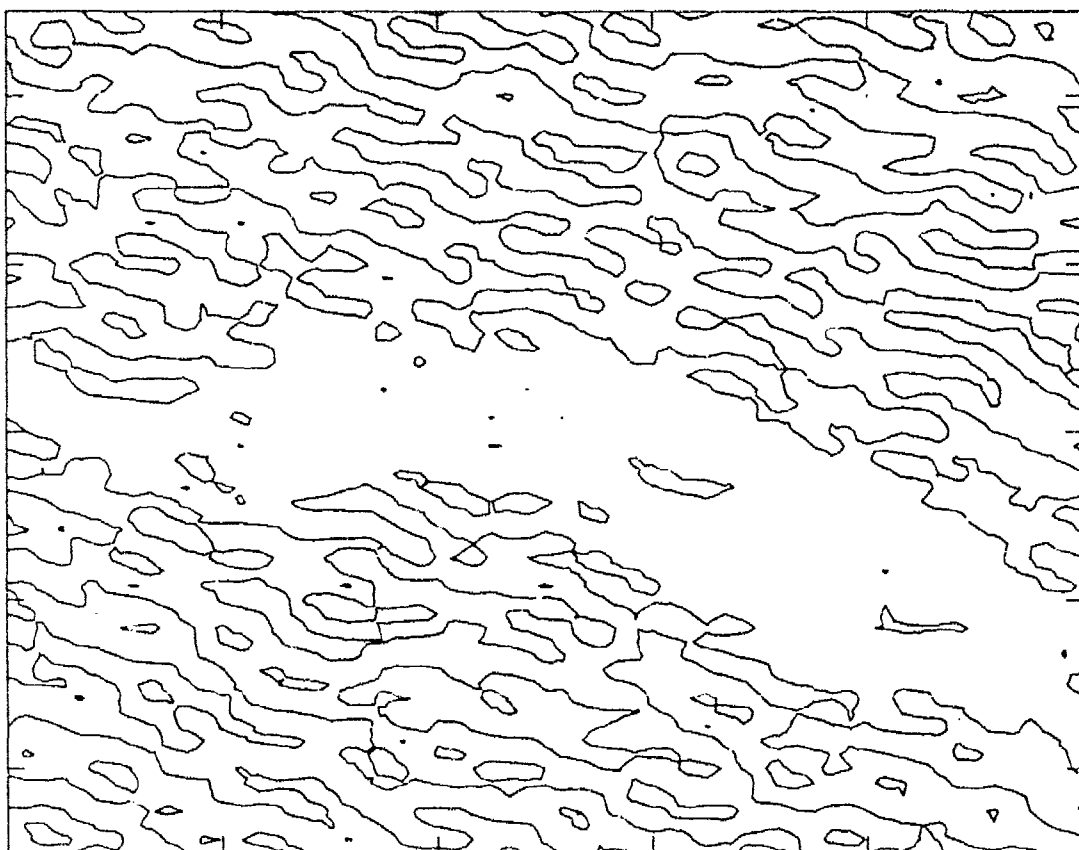
Fig. 16b — y-slope

Fig. 16 — Contour plots of superposed wave slopes for Sea State 5, $U = 0$, $\beta_W = 45$ degrees